EFFECT OF INCLINATION ON PRESSURE DROP AND FLOW REGIMES IN LARGE FLATTENED-TUBE STEAM CONDENSERS

BY

YU KANG

THESIS

Submitted in partial fulfillment of the requirements
for the degree of Master of Science in Mechanical Engineering
in the Graduate College of the
University of Illinois at Urbana-Champaign, 2016

Urbana, Illinois

Advisor:

Professor Predrag S. Hrnjak

Abstract

This thesis presents an experimental study of the inclination effect on pressure drop and flow regime during condensation of steam in a large flattened tube used in air-cooled condensers (ACC) for power plants. Steam with mass flux of about 7 kg m^{-2} s^{-1} was condensed inside a 10.7 m long, flattened test tube with inclination angle varied from horizontal up to 70^{o}. The original full-sized steel tube was cut in half along the centerline, and the removed part was replaced by a polycarbonate window to enable simultaneous flow visualization in situ with heat transfer and pressure drop measurements. A uniform velocity profile of 2.03 ± 0.12 m s^{-1} was imposed on the air side to extract heat from the steam in a cross flow direction. The experimental results showed that increasing the inclination angle led to reductions of pressure drop due to the improvement in the gravity-assisted drainage of condensate inside the test tube. At such low mass fluxes, tube inclination significantly influenced the flow pattern which was observed to be a well separated stratified flow throughout the tube at all inclination angles for downward flow. Because of the creation of the visualization window, the tube width was less than that used in industry, and thus a model that accounts for the differences in tube geometry between the full and test tube was developed and used to convert experimental pressure drop results to the full-sized tube under the same operating conditions. A prediction of pressure drop performance of the same steam condensing system under vacuum condition was also discussed. The negative dependence of pressure drop on inclination angle also prevailed in both converted results in atmospheric condition and the predicted ones in vacuum condition.

Acknowledgement

I firstly would like to express my sincere gratitude and respect to my advisor, Dr. Hrnjak, for his visionary perspectives on this research, continuous support for this project, and patient guidance of my academic life. His constant encouragements and professional advices led me to the completion of this thesis in the right direction. I would also like to offer many thanks to my lab mate, Bill Davies, whose professional comments, consistent engagement and dedicated contribution to the project brought the test facility from scratch to real, and kept patiently tutoring me for many practical aspects throughout this entire project from beginning till the end.

I would like to deeply appreciate the engineers and technicians at Creative Thermal Solution Inc. (CTS) for their professional advices and technical helps in the stage of system design and construction. Special thanks go to the fellow graduate students in the Air Conditioning and Refrigeration Center (ACRC) for their knowledge sharing in the research group and timely support whenever we were in need. I also must thank the sponsors for this project, National Science Foundation (NSF) and Electric Power Research Institute (EPRI), without their financial support, this project cannot be feasible at all. My special thanks also go to the instructors and staffs at the Department of Mechanical Science and Engineering of University of Illinois at Urbana Champaign, who inspired and offered me the knowledge that were directly or indirectly applied into this project.

Last but not least, I must offer my deepest gratitude to my parents, Yungen Kang and Aiqin Guo, who devoted themselves unconditionally and wholeheartedly in raising and educating me and encouraged me for pursing higher education oversea. I must also thank my girlfriend, Ran An, for being willing to accompany me through all the tough and good days and always experience my failures and successes together.

Table of Contents

List of Figures

List of Tables

Nomenclature

A	Cross sectional area	m^2
d	Depth	m
D_h	Hydraulic diameter	m
f	Friction factor	
g	Gravitational acceleration	$m\ s^{-2}$
G	Mass flux	$kg\ m^2\ s^{-1}$
H	Height	m
L	Length	m
$\dot{m}$	Mass flow rate	$kg\ s^{-1}$
P	Pressure	Pa
q''	Heat flux	$W\ m^{-2}$
Re	Reynolds number	
S	Perimeter	m
T	Temperature	^oC
U	Uncertainty	
V	Velocity	$m\ s^{-1}$
x	Vapor quality	
Z	Axial position: Z = 0 at tube inlet	m

Acronyms

ACC	Air-Cooled Condenser
ACRC	Air Conditioning and Refrigeration Center
CTS	Creative Thermal Solutions, Inc.

Subscripts

a	Air
b	Bulk
c	Condensate
com	Combined
ft	Full tube
$fric$	Frictional
$grav$	Gravitational

i	Interfacial
l	Liquid
mom	Momentum
0	Overall
pc	Polycarbonate
r	River
sat	Saturation
st	Steel
tot	Total
tt	Test tube
v	Vapor
w	Wall
(i, w)	Two-phase interface: vapor and liquid on the tube wall
(i, r)	Two-phase interface: vapor and liquid in condensate river

Greek Symbols

α	Void fraction	
ε	Surface roughness	mm
ϕ	Two-phase multiplier	
φ	Inclination angle	^{o}
ρ	Density	kg m^{-3}
τ	Shear stress	Pa
ω	Averaging weight factor	
χ	Martinelli parameter	

Chapter 1: Introduction

1.1 Background

The rejection of waste heat is required for most of the industrial processes. Particularly, the thermoelectric power industry rejects waste heat at a rate about twice of its electricity generation [1]. To remove the huge amount of heat out of the system, cold fresh water needs to be supplied and circulated in a secondary cooling loop. The water consumption in these thermoelectric power plants made up about 45% of the total fresh water withdrawals in the U.S. in the year of 2010 as shown in Figure 1-1. After absorbing heat, most of the used water is returned to nature at a higher temperature, which potentially increases the natural water temperature and then threatens the ecosystem downstream.

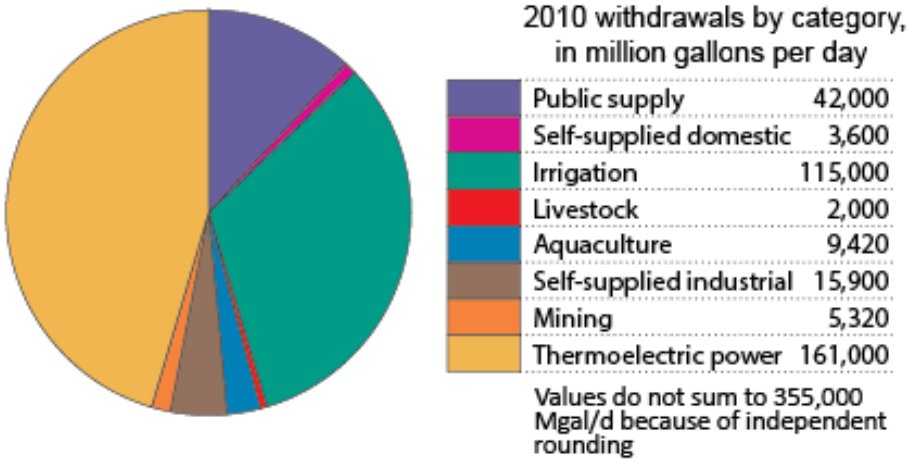

Figure 1-1 Water Withdrawals by Category in US, 2010 [2]

In addition to the environmental concerns, having long-time exposure to the wet cooling towers in the typical water cooled power plants increases the risks of contracting Legionnaires' disease, which is a respiratory infection caused by the bacteria known as legionella.

To address the above mentioned issues, the ACC system was introduced and developed

to replace the water cooling system in the traditional thermoelectric power plants. ACCs usually consist of arrays of flattened steel tubes in an A frame configuration as shown in Figure 1-2. Aluminum fins are brazed on both sides of the tube to enhance heat transfer between steam and air. Steam enters into the tube through the inlet header on top of the 'A' and exchanges heat with forced air flow induced by the axial fans at the frame base. These flattened steel tube arrays are typically installed at an inclined angle up to 60^{o} with respect to horizontal for structural stability and space reduction.

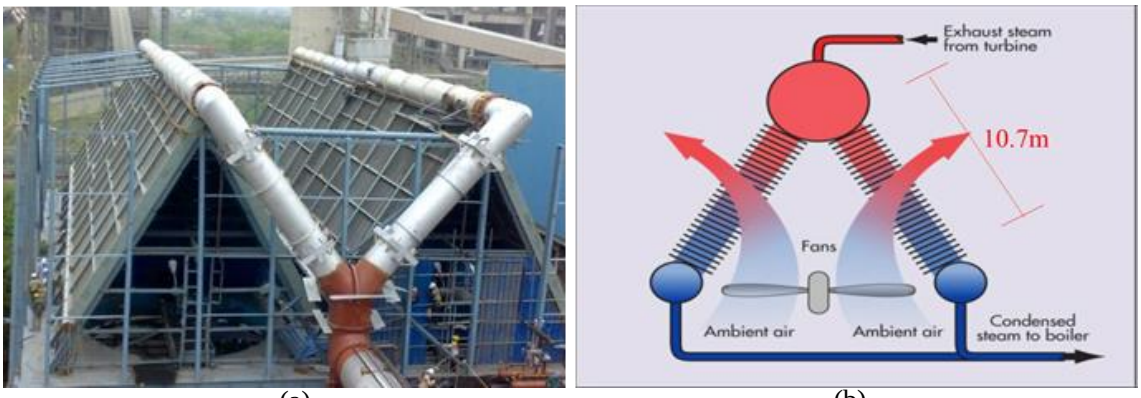

(a) (b)

Figure 1-2 (a) ACC System Installed in Power Plants (b) Schematics of ACC System

The ACC systems require zero water consumption and supply, but only 0.9% of existing thermoelectric power plant capacity in the U.S. uses such systems. Increasing the usage of ACC to 25% by 2035 would lead to a significant reduction of U.S. water withdrawal by 10.7% as estimated by the National Energy Technology Laboratory [3]. However, ACC systems provide up to 10% less power production on hot days due to a higher steam condensation temperature compared to the traditional water cooling system, and may cost up to five times more than traditional cooling tower systems. Although there are great advantages of widely adopting ACCs in the power plants, the overall efficiency of the ACC system could be further improved if heat transfer can be increased and pressure drop inside the ACC tubes can be reduced significantly.

1.2 Objectives

With the ultimate goal to enhance heat transfer and reduce pressure drop in the ACC system, this thesis is the second part of the two-part project, dealing with an experimental investigation of steam condensation inside the large flattened-tube at different inclination angles. The first part focuses on heat transfer, and this second part focuses on pressure drop and flow regime. The objective of this particular part is to characterize the two-phase pressure drop of steam condensation inside the flattened-tube at low mass flux, to correlate the experimental results with inclination angle aided by the in-situ visualizations, and to enrich the insufficient database for ACC research in flattened tubes in the open literature.

Chapter 2: Literature Review

Over the years, condensation has been well studied to account for the differences in tube geometry, working fluids and operating conditions. Many correlations were published with each improving understanding of heat transfer, pressure drop and flow regimes in the specified situations. Aiming to illustrate the theories, correlations and techniques that might be useful and applicable to this study, the following literature reviews were carried out with the emphasis on different physical aspects in the research of two-phase flow during condensation.

2.1 Two-Phase Pressure Drop and Flow Regime

Due to the high aspect ratio and low mass flow rate of steam in this study, the separated two-phase flow model tends to be more accurate in predicting the pressure drop during phase change processes as the two phases can have very different properties and velocities. Many pioneering works have been done to predict the two-phase pressure drop during condensation with a separated model for different flow regimes and conditions. However, most of the correlations can only be applied over a limited range of conditions.

Lockhart and Martinelli [4] proposed the methods for determining the two-phase multipliers ϕ_l and ϕ_v in the separated model. Based on these two-phase multipliers, the frictional pressure drop can be predicted for isothermal flow in a horizontal round tube. Chisholm and Laird [5] later formulated the two-phase multipliers with a constant C and Martinelli parameter χ as

$$\phi_l = \left(1 + \frac{C}{\chi} + \frac{1}{\chi^2}\right)^{1/2} \tag{1}$$

$$\phi_v = \left(1 + C\chi + C\chi^2\right)^{1/2} \tag{2}$$

These works established the foundation for analytically predicting pressure drop for two-phase flows in the phase change processes, and many other subsequent correlations were modified or developed based on these first widely applicable studies. One of the examples is the Friedel [6] correlation for predicting two-phase multiplier $\phi_{l,o}$ in a round tube for vertical upward and horizontal flow according to the database of 25,000 data points. The detailed reviews and formulations of this correlation are given in [7].

In addition to the above mentioned generic but fundamental two-phase pressure drop correlations, some other separated flow models were specifically developed for certain flow regimes. Taitel and Dukler [8] developed the pressure drop model for smooth, equilibrium stratified flow by momentum balance on each phase, and the model can be written as

$$-A_l\left(\frac{dP}{dx}\right)-\tau_{w,l}S_l+\tau_i S_i+\rho_l A_l g\sin\varphi=0 \tag{3}$$

$$-A_g\left(\frac{dP}{dx}\right)-\tau_{w,g}S_g+\tau_i S_i+\rho_g A_g g\sin\varphi=0 \tag{4}$$

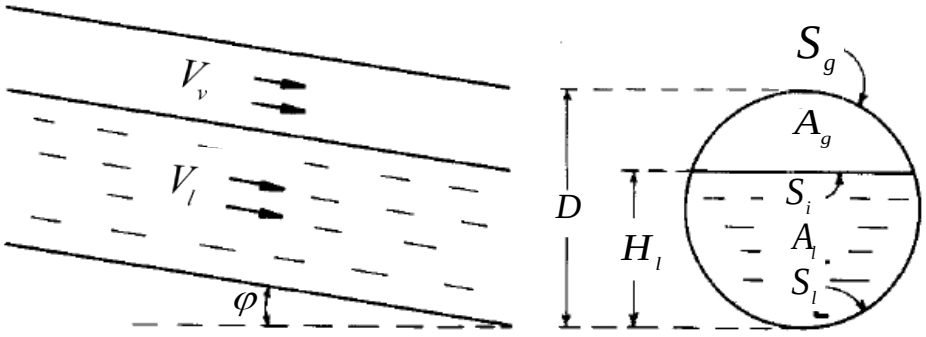

Figure 2-1 Stratified Two-Phase Flow Geometry Considered by Taitel and Dukler, adopted from [8]

The evaluation of the shear stresses in Equation (3) and (4) requires the determination of wall and interfacial friction factors, and some efforts have been made to correlate the

friction factors with measurements. Kowalski [9] presented experimental results for wall and interfacial shear stresses in the stratified flow using wall shear stress and void fraction measurements. The wall shear stress measured with a hot-film anemometry technique helped the determination of the interfacial shear stress and an empirical correlation for the interfacial shear stress in smooth stratified flow was proposed as

$$f_i = 0.96\left(\mathrm{Re}_v^+\right)^{-0.52} \tag{5}$$

where Re_v^+ is the superficial vapor Reynolds number.

Ouyang and Aziz [10] developed the empirical correlations for the prediction of wall and interfacial friction factors in stratified flow based on large amounts of experimental data. This data regression based correlation was reported to have a good agreement with other experimental results, but the missing mechanistic explanations introduced some discontinuities around the flow pattern transition boundaries.

More detailed reviews for pressure drops in other flow patterns are presented in [7], [11], and [12], and are not elaborated here.

2.2 Pressure Drop and Flow Regime in Non-Circular Tubes

Many correlations have been published for predicting two-phase pressure drop and void fractions in circular tubes, but few were for the tubes with non-circular cross section. Sadatomi and Sato [13] conducted experimental research on two-phase pressure drop and flow regimes in vertical upward flow in noncircular channels. The modified Reynolds number by employing the means of a geometry factor for non-circular channels was reported to have better agreement with experiment data compared to the common approach of redefining hydraulic diameter for different geometry in single phase. Using the newly defined Reynolds number to calculate frictional pressure drop in each phase,

the two phase multipliers in the Chisholm & Laird [5] correlation were determined, and such an approach was said to be applicable to correlate two-phase pressure drop in noncircular channels. Flow visualization in this study also showed that the two-phase flow pattern transition was not remarkably influenced by the channel geometry when hydraulic diameter is greater than about 10 mm.

Two-phase pressure drop was also studied by Ide and Matsumura [14] in rectangular channels at different inclination. Their experimental results showed that neither the Lockhart-Martinelli [4] nor Akagawa [15] correlation worked for accurately predicting pressure drops in the rectangular channel at large inclination angles and low superficial liquid velocity. An empirical correlation based on separated flow analysis was proposed to correct the two-phase multiplier ϕ_l in pressure drop calculation after incorporating the effects of aspect ratio of the channel geometry and the inclination angle. The experimental results showed an agreement with the correlation with an accuracy of ±30%.

Wambsganss et al [16] have conducted very comprehensive experimental studies on two-phase pressure drop in a small horizontal rectangular channel for the total mass flux ranging from 50 to 2000 kg m^{-2} s^{-1}. As was supported by their experiment data, the accuracy of the prediction by the Chisholm and Laird [5] correlation depended strongly on mass flux, and can be very poor if a constant value of C was used for all the mass flux range tested in this study. Friedel correlation [6] was also compared with experiment data, but systematic errors were appeared as a function of mass flux. Further investigation showed that C was not a constant for mass flux less than 400 kg/m^2s, but a function of Martinelli parameter χ and mass flux instead. An empirical equation was proposed to explain such a relationship, and the modified Chisholm and Laird correlation with such corrected C values provided better predicted results with an average error of less than 19%.

Similar studies were carried out by Lee and Lee [17] to look into the pressure drop correlations for two-phase flow in horizontal rectangular channels with narrow gap. The channel had longer width than height, which is opposite to the flattened tube used in this study. The classical Lockhart-Martinelli correlation with constant parameter C failed in representing experimental data, and thus a modified C that varied according to different mass flow rate and gap size of the channel characterized by hydraulic diameter was proposed. The exact expression of C value relied on empirical data regression. The correlation was validated by the measurements from Mishima et al [18] within 10%, and from Wambsganss [16] et al within 15%.

In addition to the research on adiabatic air-water two-phase pressure drop and flow regime, other studies have also focused on the two-phase pressure drop and flow regime in non-circular tubes during condensation. Coleman & Garimella [19] investigated flow regimes in round, sqaure and rectangular tubes during condensation of R134a. A very comprehensive flow regime map was proposed for the condensation of R134a in different tube geometries, and was compared with existing results in the literature. Their visualiation results showed that flow regime transitions were not very strongly dependent on tube shape and aspect ratio for the tubes with similar hydraulic diameters, but such transition can be greatly influenced by the difference in hydraulic diameter.

Wilson et al [20] experimentally studied two-phase pressure drop of refrigerant condensation in round and flattened tubes. By successively compressing and deforming the round tubes, flattened tubes were made with the same cross sectional area but smaller hydraulic diameter compared to its original round ones. The experimental data showed that pressure drop increased at a given mass flux and quality as tube profile was flattened, but heat transfer was enhanced at the same time. Additionally, significant reduction in refrigerant charge was achieved if a tube was flattened. Their pressure drop data fell

within ±20% error as the prediction by Jung and Radermacher [21].

Most recently, Kim et al [22] confirmed the limited availability of relevant research on condensation in a flat tube in the literature, and conducted an experimental investigation on heat transfer and pressure drop in flattened tubes during the condensation of R410a. As discovered by their data, pressure drop always increased as aspect ratio became larger. The accuracy of predicting pressure drops from different correlations depended on the selection of hydraulic or equivalent diameter. A reasonable prediction of two-phase pressure drop was discovered using the Muller-Steinhagen and Heck [23] correlation with hydraulic diameter, and the Friedel correlation with equivalent diameter.

2.3 Pressure Drop and Flow Regimes in Inclined Tubes

Tilting the heat exchanger tube at different inclination angles changes flow patterns and thus influences heat transfer and pressure drop, but few studies are available to investigate the effect of tilting angle on heat transfer and pressure drop during condensation [24].

One of the early studies from Beggs and Brill [25] found out that several acceptable correlations for predicting pressure drop and liquid holdup in horizontal or vertical flows cannot be successfully applied to the inclined flow. Varying the inclination of two 45-foot-long acrylic pipes, air-water pressure drop and liquid hold-up were recorded. The results showed that in downwardly inclined flow, the flow pattern was almost separated and the liquid holdup decreased as the angle increased in the negative direction. However, after about 60^{o}, the flow pattern changed to annular and an increase in viscous drag offset the increase in gravitational force which led to the decrease in liquid velocity and an increase in liquid holdup. An empirical correlation that involved inclination angle and flow rate of each phase was developed to predict the liquid holdup inside the tube for different flow regimes. Friction factor for two-phase pressure drop was also correlated

empirically as a function of liquid holdup, liquid content (the ratio of liquid volumetric flow rate to total volumetric flow rate) and Froude number.

Andreussi and Persen [26] studied the two-phase pressure drop and liquid holdup for stratified flow in downwardly inclined pipes. A flow map specifying transitions between stratified smooth, wavy and slug flow in a lightly inclined (0.65^o and 2.1^o) tube was built based on the experimental data. Such transitions in flow regime brought changes in interfacial shear, and thus a step-wise interfacial friction factor corresponding to the sub-regimes in stratified flow was proposed. And liquid holdup was found to be only affected by liquid Reynolds number and liquid friction factor.

A more comprehensive study done by Lips and Meyer [27] provided detailed experimental results of pressure drop during the condensation of R134a in a round tube for a whole range of inclination angles. Experimental results discovered that, at contant mass flux, pressure drop increased as inclination angle increased in the upward direction and decreased as inclination angle increased in the downward direction, compared to the pressure drop at horizontal. The decreasing trend of pressure drop in the downward flows was less significant than the increase in the upward flows. Pressure drop and void fraction data were also compared with existing correlations for horizontal and vertical orientations. Data for the slightly inclined orientation for downward stratified flows were compared with Taitel and Dukler's [8] model, and was proven to be successful. However, further studies are needed to correlate pressure drop and void fraction at inclined conditions.

Most recently, Adelaja et al [28] published the experimental study of pressure drop during condensation in an inclined tube with focus on varying saturation temperatures. A similar trend of pressure drop when changing inclination angle was discovered as that in [27]. The results proved that shear force was the dominant factor in influencing pressure drop for high mass fluxes and qualities, but gravitational force that originated from the

inclination effect was dominant for low mass fluxes and qualities. Additionally, affected by the inclination, flow regime transitions for upward and downward flows were stated to be very different. Such differences led to the changes in frictional pressure drop at different inclination angles. However, no direct void fraction measurements were provided in this study, but reasonable predictions using existing correlations were compared with pressure drop data, and the dependence of such predicted void fraction on inclination angle was also discussed.

2.4 Pressure Drop in Air-Cooled Condenser

The application of ACCs in the power generation industry has been a well-studied subject over the years. As one of the natural draft dry cooling system, air-cooled heat exchanger design and performance evaluation were comprehensively discussed in the pioneering works done by Kröger [29]. The main focuses of the past research about the ACC systems were on the characterization and optimization of air-side heat transfer and pressure drop performances, such as the effect of air-flow maldistribution, wind effects, non-uniform temperature profiles and other drawbacks. A detailed investigation into the performance of a power plant with an air-cooled condenser was discussed by O'Donovan and Grimes [30].

Very limited research has focused on steam-side pressure drop in the air-cooled condenser tubes. Most recently, O'Donovan and Grimes [31] conducted an experimental study on steam-side pressure drop in a full-scale ACC circular tube bundle under vacuum conditions. Operating at the mass fluxes between 0.7 to 2 kg m^{-2} s^{-1}, the measured pressure drop between inlet and outlet header was relative small, in the range of 130 to 250 Pa. However, the momentum recovery originated from phase change was reported to be considerably large, with a range from about 2 to 12 kPa. Such a large momentum recovery was mainly due to the high vapor velocity at the vacuum condition, which in turn implied

a large frictional pressure loss inside the tube during condensation as frictional pressure drop was calculated by subtracting momentum and gravitational pressure drop from measured total pressure drop. Such phenomena have not been validated by other researchers yet mainly because of the lack of existing research on the same topic. The experimental results were also compared with several well-established correlations, and the prediction from Lockhart-Martinelli correlation gave the best agreement within ±20% error. The inclination angle was not varied but kept as a common value in the A frame air-cooled condensing unit.

All the above mentioned existing studies provided very detailed illustrations and helpful results that inspired ideas and references for this research. However, none of them have looked into the influence of pressure drop from combined factors such as low mass flux, non-circular tube geometry and inclination angle together. To fill such a gap in literature, this experimental investigation focused on studying two-phase pressure drop during the condensation of steam in a non-circular, flattened tube at various downward inclination angles.

Chapter 3: Experiment Setup

3.1 Facility Overview

A schematic drawing of the experimental facility is shown in Figure 3-1. Steam was provided by two boilers running in parallel with capacities of 27 kW and 24 kW respectively. The boiler powers were individually controlled by solid-state controllers so that the mass flux of steam could be properly adjusted. An inlet heater and a gate choke valve were installed before the steam inlet header to ensure slightly superheated steam entering into the system. At the outlet of the condenser, a condensate pump acting as a receiver collected liquid water and pumped it back to the boiler when the pump filled, forming a closed-loop system.

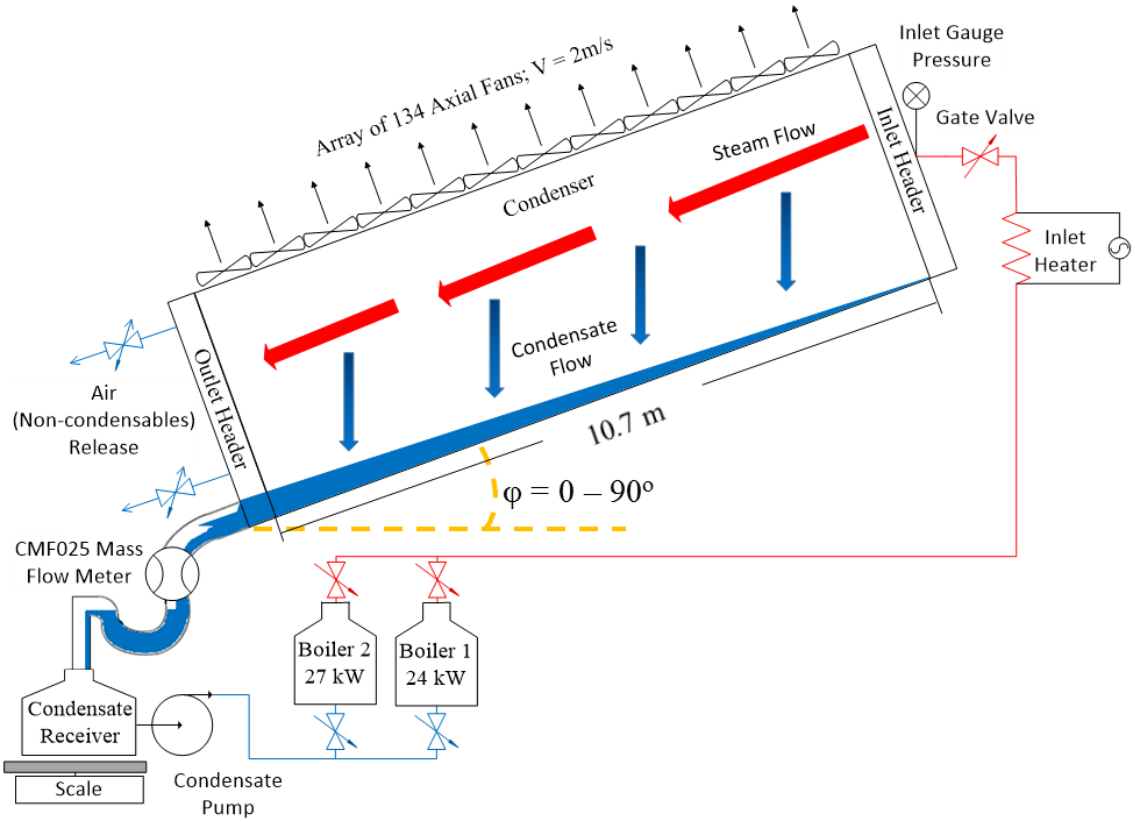

Figure 3-1 Schematic Drawing of the Experiment Facility

The condenser was essentially a type of cross-flow heat exchanger, with steam flowing along the tube length direction and air flowing perpendicularly with respect to steam flow. Steam condensed inside the 10.7 m long flattened tube, the same length as the actual condenser tubes in ACC power plants. Air flow provided by 134 axial fans with diameter of 80 mm on top of the condenser tube extracted heat out of the steam. The fan speeds were adjustable individually via 1 kΩ potentiometers. The entire condenser tube assembly was attached to a rigid truss so that the experimental setup was capable of varying inclination angles from horizontal up to 70^{o} as shown in Figure 3-2. Due to the large scale of the facility and the limited height of the lab ceiling, a large portion of the experimental works were conducted outside of the room with the help of a heavy duty fork lift as shown in Figure 3-3.

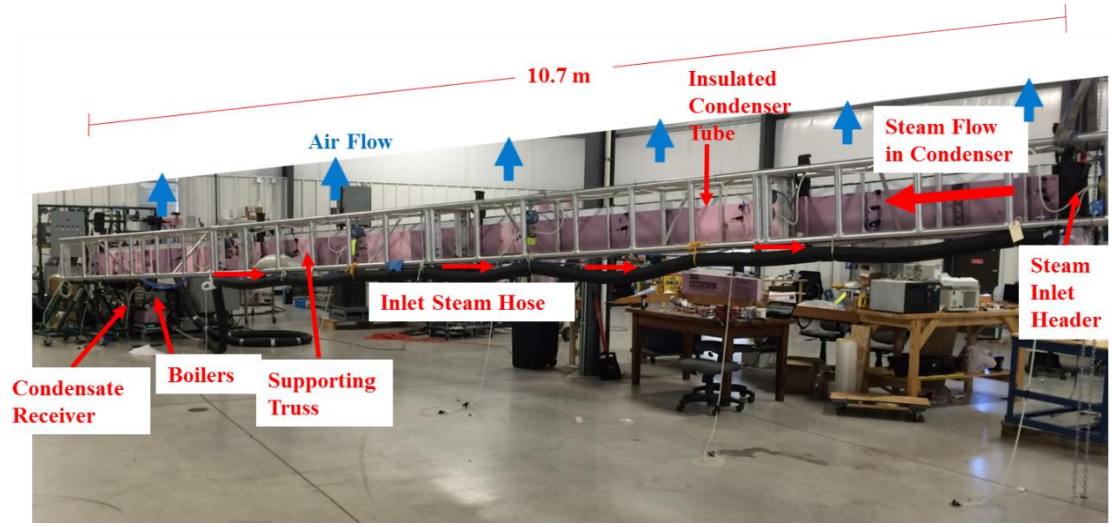

Figure 3-2 Experimental Setup

Figure 3-3 Experimental Setup Outside

3.2 Large Flattened Tube: Full-Size Tube and Half-Size Test Tube

The condenser tubes in the ACC system in power plants typically have the dimensions of 10.7 m in length, 0.214 m in height and 0.02 m in width. The cross section view is shown in Figure 3-4. Such flattened and externally aluminized steel tubes with fins brazed on have good performance characteristics, and are well suited for ACC systems where only one row of these tubes is placed instead of multiple rows of round or elliptical tubes [29].

For this experimental study, the original flattened tube was cut in half and a polycarbonate window replaced the removed part, forming a half-size test tube, as is illustrated in Figure 3-5(a). Such a half-tube design complicated the interpretation of the pressure drop measurements by removing the direct applicability of the experiment results to the pressure drop in a full-sized power-plant condenser tube. However, such a sacrifice was

paid off by having clear visual access to the flow regimes along the entire length of the condenser tube and at different inclination angles, which enabled the measurements of void fraction simultaneously with heat transfer and pressure drop data recording. Flow patterns, and their alterations with inclination angle, have a strong influence on the two-phase pressure drop, therefore it is essential to work with such a design. Nonetheless, special attention must be paid to accurately predict the pressure-drop performance of the actual condenser tube, and hence a model to relate the pressure drop measurement in the test tube to full tubes was developed and elaborated in Section 5.1.

Air flow was constrained inside an air duct, and 2-inch-thick insulation foam was attached on the air duct. The same foam insulation was also attached to the polycarbonate window so that an adiabatic condition on the polycarbonate side could be maintained when not doing visualization. Figure 3-5 (b) shows the cross section of the final assembly of the test tube.

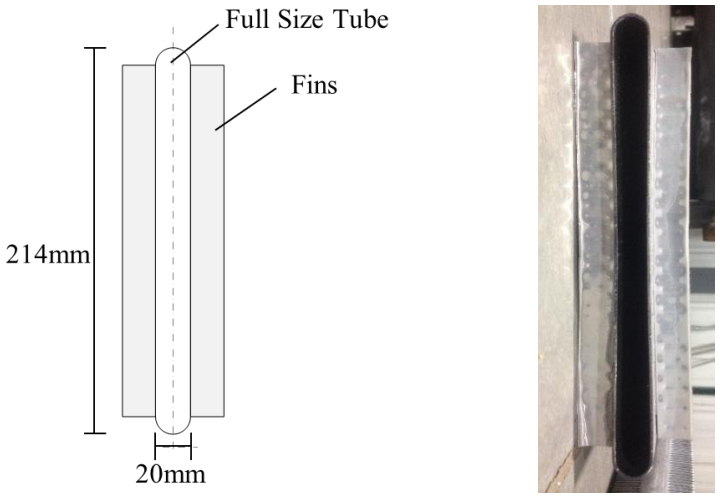

(a) (b)

Figure 3-4 Cross-sectional View of Full-Size Flattened Tube: (a) Schematic, (b) Actual Photo

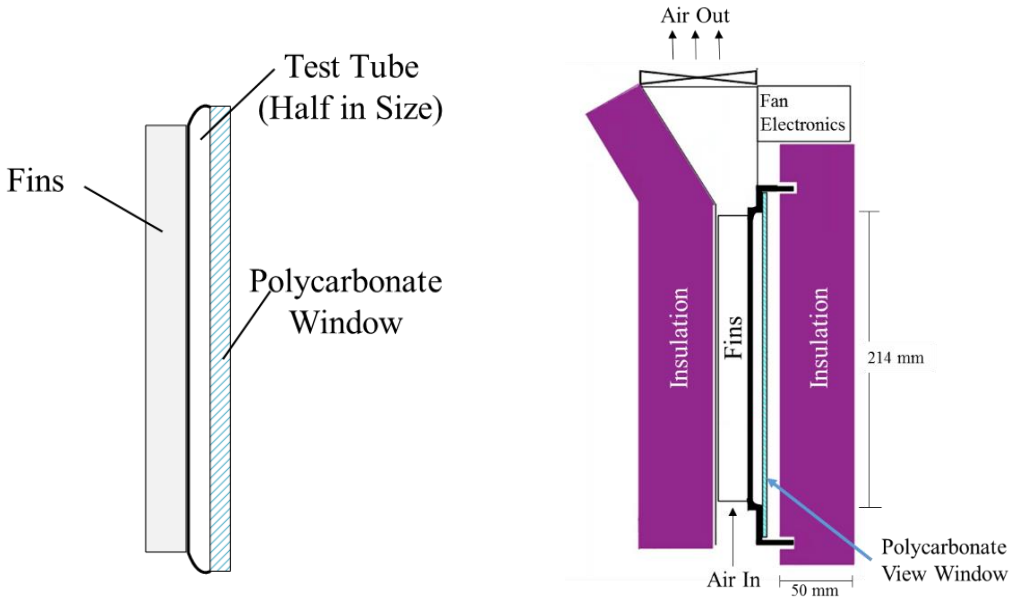

(a) (b)

Figure 3-5 Cross-Sectional View: (a) Half-Size Test Tube, (b) Test Tube Assembly

3.3 Instrumentation

Figure 3-6 illustrates the arrangement of sensors along the tube and their relative locations in the cross section.

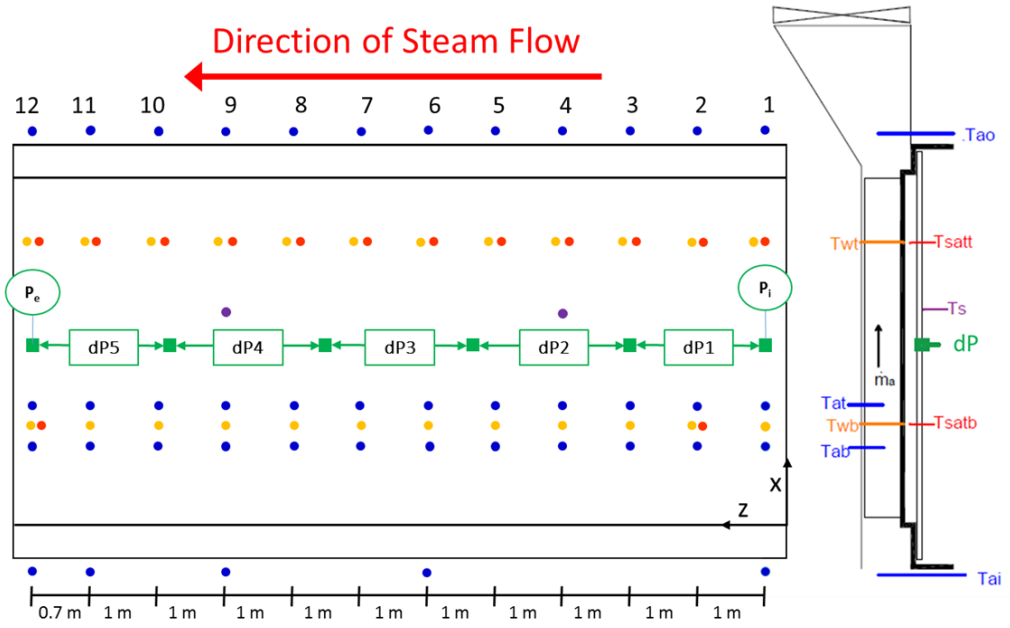

Figure 3-6 Schematic Drawing of Sensor Arrangement

Along the tube, five equally spaced pressure drop measurement sections were developed to record pressure drop data on the steam side by Rosemount® differential pressure transducers. During condensation, steam velocity decreased from the maximum value of about 11 m s^{-1} at the inlet to stagnant at the exit, and thus pressure sensors with larger range were selected closer to the inlet and smaller ones near the outlet for accuracy. Gauge pressures at inlet and outlet were also measured by two additional differential pressure transducers. Atmospheric pressure was recorded from a locally installed mercurial barometer. All the sensors were calibrated within 1% against a standard manometer after mounted onto the system. The full ranges of the five differential pressure sensors were selected to be 2 inH_2O (497.68 Pa), 1 inH_2O (248.84 Pa), 1 inH_2O (248.84 Pa), 0.5 inH_2O (124.42 Pa), and 0.35 inH_2O (87.097 Pa), respectively for dP1 to dP5.

Pressure sensors with such small ranges were very sensitive to orientation. In order to accurately measure pressure drop variations as inclination angle changes, a fixture with a simple shaft-and-bearing mechanism, as shown in Figure 3-7, was designed and installed on the truss so that the attached pressure sensors can stay vertical by gravity regardless of tube inclination.

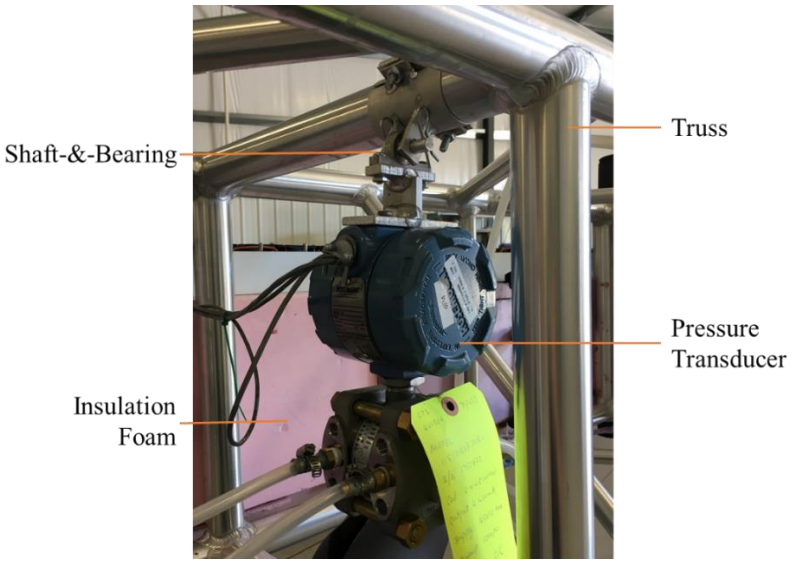

Figure 3-7 Pressure Sensor Mounting Mechanism

To avoid condensate being trapped inside the pressure hose, a Y connection was used for every pressure drop measurement station. As shown in Figure 3-8, any condensate in the pressure hose was drained down by gravity to the lower end through the Y connection so that a non-blocking connection between pressure sensor and the port on the tube for pressure drop measurements was ensured.

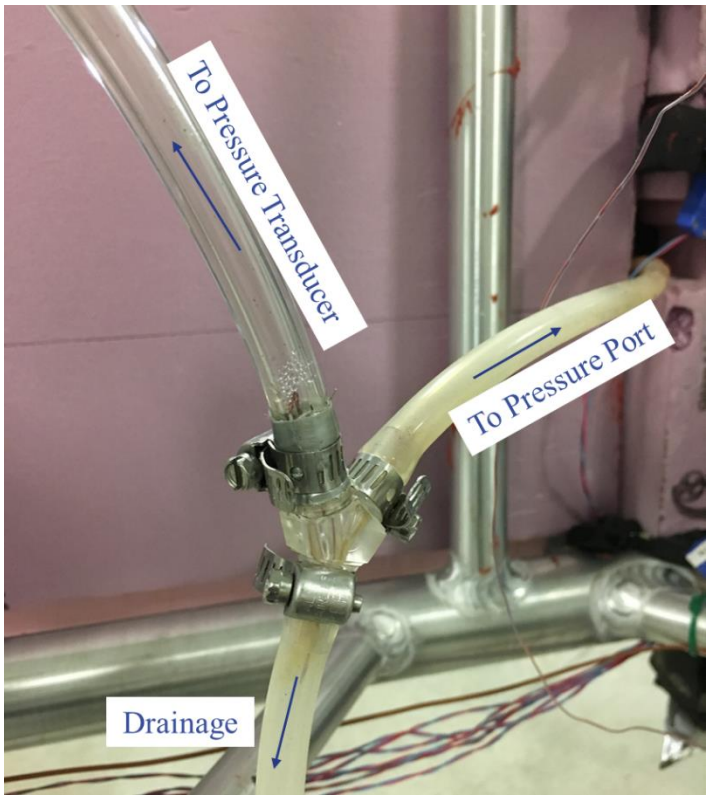

Figure 3-8 Y Connection between Pressure Transducer to Measurement Port

Condensate mass flow rate was recorded by a Micro Motion® CMF025 Mass Flow meter at the exit of the condenser tube. A digital scale was also used as a redundant measurement of condensate mass flow rate by recording the changes in condensate weight against time change. For accuracy and convenience, the digital scale measurements were used only for checking measurement consistency. The mass flow meter was calibrated using the "bucket and stopwatch" method on the calibration facility at CTS.

Twelve sets of temperature measurements were recorded at 1 m interval along the tube, as indicated in Figure 3-6. At each measurement station, one set of temperatures, which included two steam saturation temperatures, four air-side temperatures, and two wall temperatures, was recorded by calibrated T-type thermocouples for calculating heat fluxes, vapor qualities, and heat transfer coefficients. The instrumentation and determination of heat transfer data were elaborated in detail in the counterpart of this project [32].

3.4 Test Conditions

In-tube pressure drop was measured at various inclination angles in the test tube. Due to the large scale of the experiment setup and limited structural support at higher inclination angles, the inclination angle of the test tube was able to be varied from horizontal up to a maximum of 70°. To eliminate possible errors caused by sun light radiation during the day, the experimental tests were conducted in the night. The experimental results were obtained under the conditions listed in Table 3-1.

Table 3-1 Test Conditions

Parameter	**Range**	**Uncertainty**
Inlet vapor mass flux [kg m^{-2} s^{-1}]	6.2 – 7.5	± 0.1
Mass flow rate of condensate [g s^{-1}]	9.2 - 10.6	± 0.1
Condenser capacity [kW]	25.2 – 29.1	± 3%
Air velocity (average) [m s^{-1}]	2.03	± 7%
Vapor inlet pressure [kPa]	102 – 106	± 0.1
Vapor inlet superheat [°C]	0.1 – 0.7	± 0.05
Inclination angle [°]	0 – 70	± 0.5

Chapter 4: Flow Visualization and Discussion

Although exact heat transfer and pressure drop measurements in the actual condenser tube are important, the physics behind the phenomena are usually unclear when flow interactions and regimes are not able to be visualized nor characterized. As was illustrated in Chapter 3, the great advantage of this facility is its capability of visualizing flow patterns and recording heat transfer and pressure drop data on the same facility at the same time. Although the surface of the test tube was gradually rusted while full condenser tube operating in an ACC system may experience less rusting as non-condensables are constantly removed under vacuum condition, the effect of such difference is expected to be small as the full tubes must have certain extent of rusts due to the presence of non-condensables. However, the cleanliness of the full tube cannot be visualized and confirmed. Therefore, the observed flow regimes inside the test tube are assumed to be identical to the full tube in an ACC system. Such a direct indication of flow patterns was provided and reproduced in the test tube by controlling its inlet steam velocity and mass flux to be the same as they are in a full tube. The results of flow visualization are discussed here in this chapter.

4.1 Flow Pattern and Liquid Holdup at Different Inclination Angles

As is demonstrated in Figure 3-1, the high aspect ratio of the flatted tube and low mass flux of steam resulted in a very separated two-phase flow pattern. Steam flowed axially and decelerated from the inlet to the outlet. Condensate was formed on the steel tube wall, with a mixed mode of both filmwise and dropwise condensation as is depicted in Figure 4-1, and slid down by gravity to the river on the bottom. The river was accelerated by vapor shear and gravity while collecting the falling condensate downstream along the tube, and finally drained out. Although this general description of the flow pattern was observed to be universal in all inclination angles, certain distinctions were evident

between horizontal and inclined situations.

Figure 4-1 Illustration of Mixed Mode Condensation (30° inclination, Z=6.4 m)

4.1.1 Horizontal Vapor and Condensate Flow

When tube was horizontal, the falling droplets and film were pushed away from their vertical path down along the wall by the turbulent vapor flow. The high vapor velocity near the inlet generates a wavy interface between vapor and condensate river, and such a flow pattern is demonstrated in Figure 4-2 and Figure 4-3. The heavy interactions between vapor and condensate near the entrance created large energy loss in the flow, and thus the pressure drop was the highest in this region compared to the others downstream.

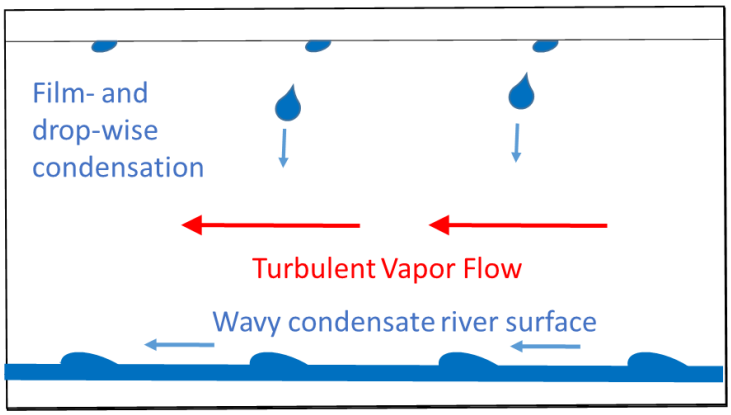

Figure 4-2 Demonstration of Wavy Condensate near the Entrance (used with permission from [32])

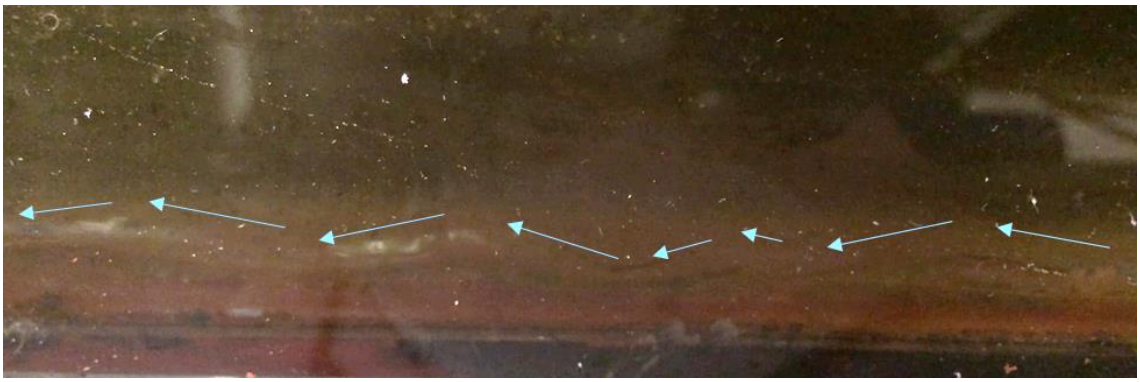

Figure 4-3 Wavy Condensate River near the Entrance (used with permission from [32])

As vapor velocity decreased due to condensation and friction, gravity became the dominant force for the falling droplets and film. The condensate on the steel wall then slid down along the wall vertically and merged into the condensate river. The wavy river interface disappeared after about 2 m away from the inlet, but the liquid holdup increased dramatically as no effective drainage was provided by gravity, as shown in Figure 4-4. At horizontal, vapor shear was the only driving force to push condensate river flow downstream before the liquid was held to a critical level of about 22 mm as shown in Figure 4-6. This critical level is an indication of the balance between vapor shear and gravity force on the condensate river, after which the condensate river becomes a free over-fall dominated by gravity only.

Close to the exit, nearly quiescent vapor was condensed. Although heat transfer results indicated zero quality near the exit [32], the tube was not fully filled with liquid due to the non-equilibrium thermodynamic condition during the condensation process in this flattened tube. The condensate near the exit was subcooled because the location of the condensate river at the tube bottom corresponded to the location of the lowest air temperature.

In this horizontal tube, the two-phase flow was consistently separated throughout the tube with some small variations due to the difference in vapor velocities along the tube.

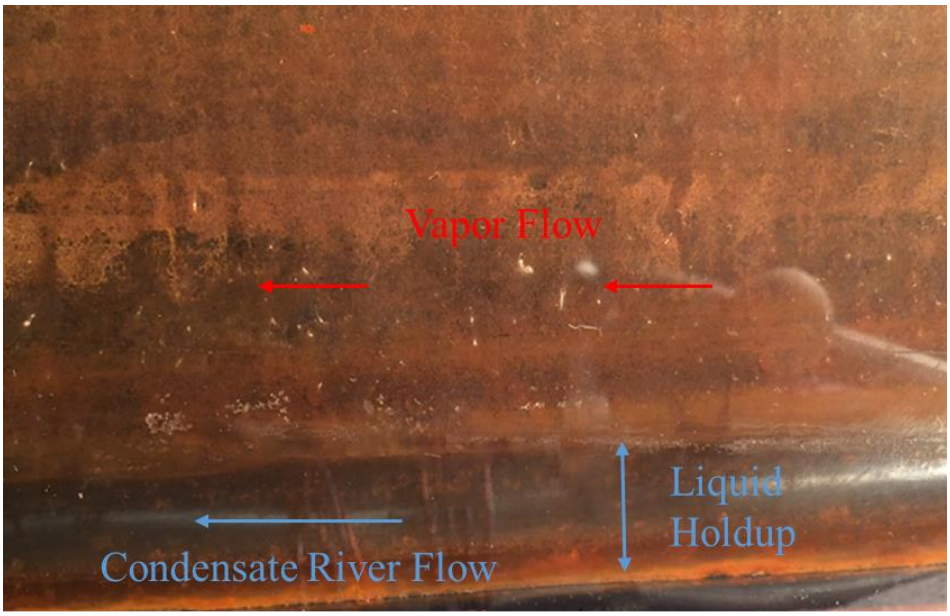

Figure 4-4 Flat Vapor and Condensate Interface (Horizontal, Z = 10.3 m)

4.1.2 Inclined Vapor and Condensate Flow

As inclination angle increased, the influence of gravity on flow pattern increased accordingly while the well-separated liquid and vapor flow pattern was still dominant.

When tube was inclined, the liquid film and droplets fell down along the tube surface in a nearly vertical downward direction, except near the first few meters near the tube entrance where vapor shear prevented the condensate from falling straight down, regardless of tube inclination. With increased inclination angle, the path for condensate to fall before merging into the river was lengthened, as illustrated in Figure 4-5, and thus the average velocity of condensate on the wall increased. However, the film was very thin on the steel surface, less than 0.1 mm based on Nusselt's analysis, and the density of liquid is about 2,000 times larger than the density of vapor, the inertia of the liquid on the wall became so significant that the liquid cannot be accelerated to a very high velocity as vapor can. So even at large inclination angles, the slightly higher velocity of liquid film and droplets cannot cause more significant energy losses.

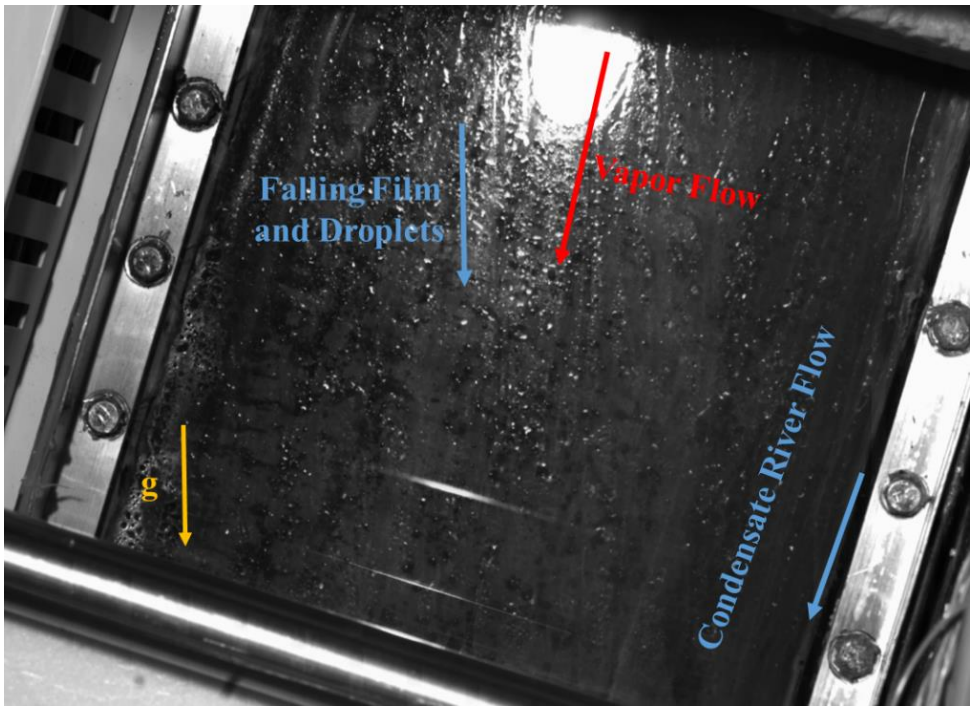

Figure 4-5 Vapor and Condensate Flow at High Inclination Angle (70^{o} inclination, Z = 10.5 m)

At inclined condition, the wavy condensate river completely disappeared in inclined tubes. The condensate cannot accumulate near the entrance region due to the gravity-assisted drainage. Instead, the condensate river depth became comparably smaller when the tube was inclined downwardly in contrast to the thick river depth at horizontal. Moreover, the hump observed in horizontal tube disappears when tube was inclined even at 3^{o} as shown Figure 4-6. Along the axial direction, depth of the condensate river increased as the condensate formed in the downstream joins into the river. Such a profile of condensate river depth indicated that vapor shear did not have any significant effects on the flow of condensate river, but gravity did in the entire tube. At each measurement location, the depth of the condensate river became thinner and thinner as inclination angle increased. All these phenomena proved the significance of gravity over shear in influencing the flow patterns in the inclined conditions.

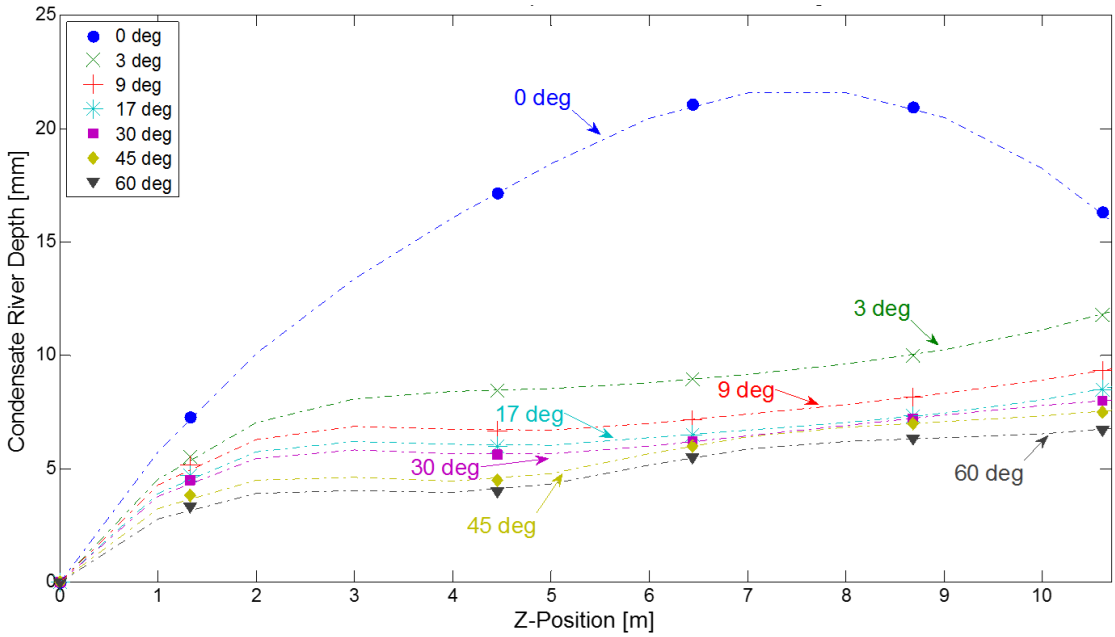

Figure 4-6 Depth of Condensate River at Different Angles along the Tube

4.2 Void Fraction Measurement and Modeling

The void fraction of two-phase flow was determined from the measurements of condensate river depth as shown in Figure 4-6. The cross-sectional area of the condensate river A_c was calculated from the river depth measurements based on the test tube geometry [32], and then the void fraction was obtained from

$$\alpha = \frac{1 - A_c}{A_{tot}} \tag{6}$$

where A_{tot} is the total cross-sectional area of the test tube. In this calculation, the volume occupied by the condensate film and droplets on the steel wall were neglected because the film thickness was very small, less than 0.1 mm based on Nusselt's analysis. The results of void fraction measurements are shown in Figure 4-7.

Notice that the y-axis of Figure 4-7 was not started from 0 as the void fractions were consistently large in all inclination angles. Even near the exit where the bulk vapor quality

was found to be 0, the void fraction was still above 0.9, which suggested a very strong non-equilibrium thermodynamic conditions in the two-phase flow.

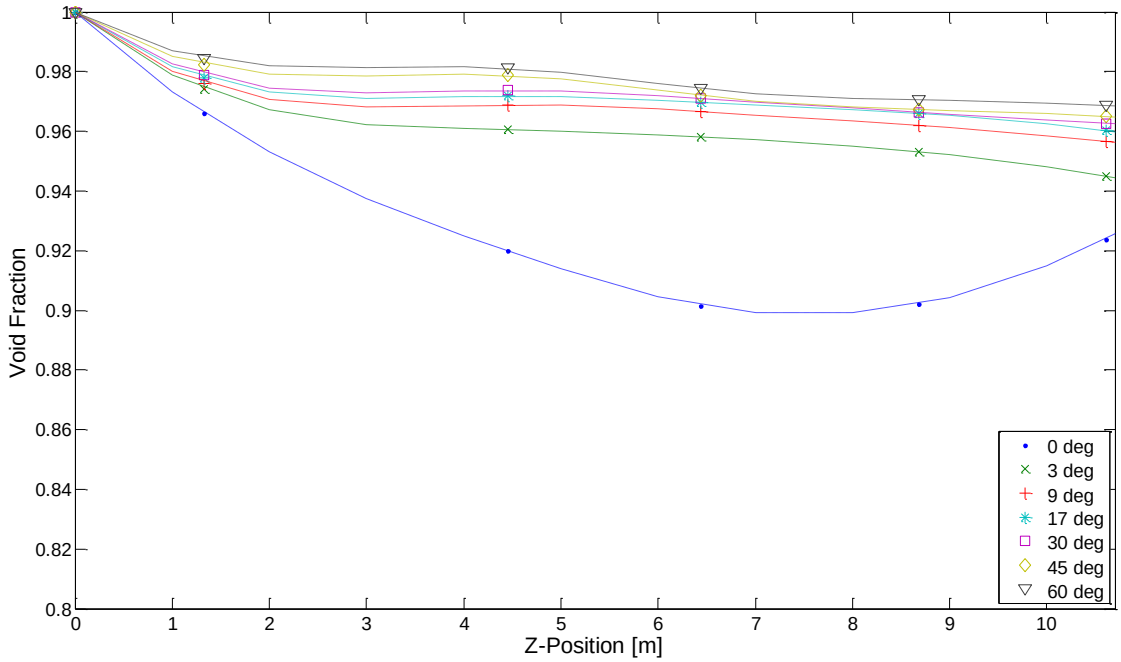

Figure 4-7 Void Fraction Variation along the Tube at Different Inclination Angles

As the majority of existing void fraction correlations uses bulk quality as model input, the predicted void fraction is always 0 at quality of 0. However, these correlations are not applicable to a thermodynamically non-equilibrated system in which void fraction is non-zero at bulk quality of 0. An example of the inconsistency in void fraction measurements and predictions from Thom [33], Baroczy [34], Lockhart and Martinelli [4], Zivi [35] and Wallis's [11] at 45^{o} inclination is illustrated in Figure 4-8. A comparison of all measured void fraction and predictions from the same resources was plotted in Figure 4-9, in which systematic errors occurred for all correlations when void fractions were predicted to be 0 while the measured ones were around 0.95. So it is improper to obtain actual void fraction inside the test tube with these traditional correlations.

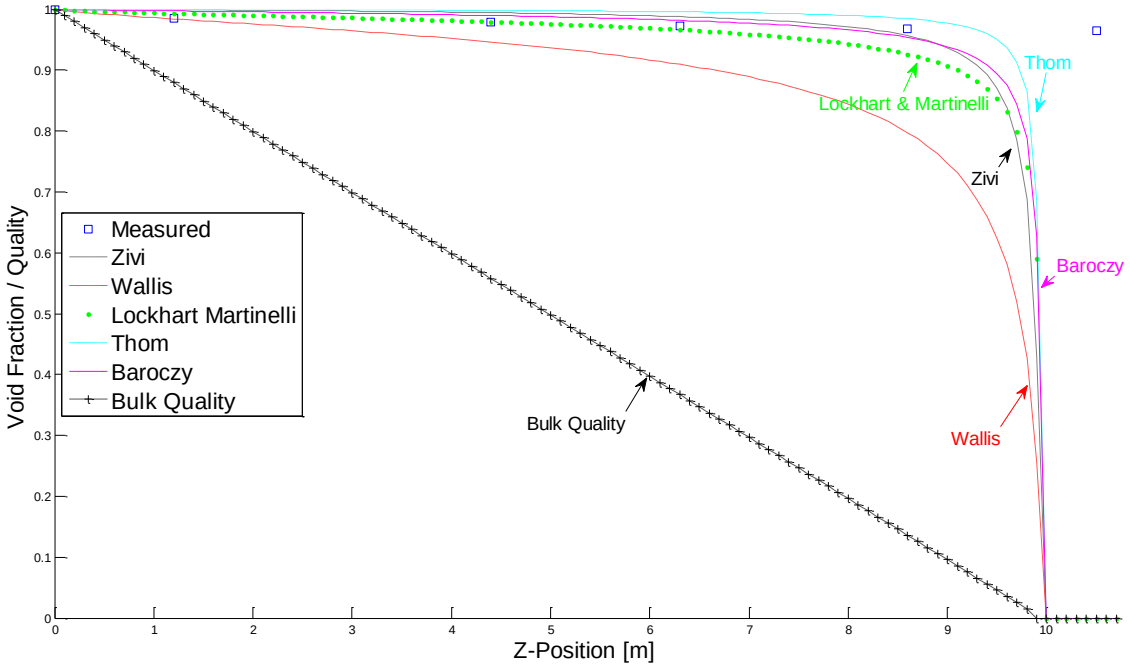

Figure 4-8 Void Fractions along the Tube at 45°: Measured vs Predicted by Bulk Quality

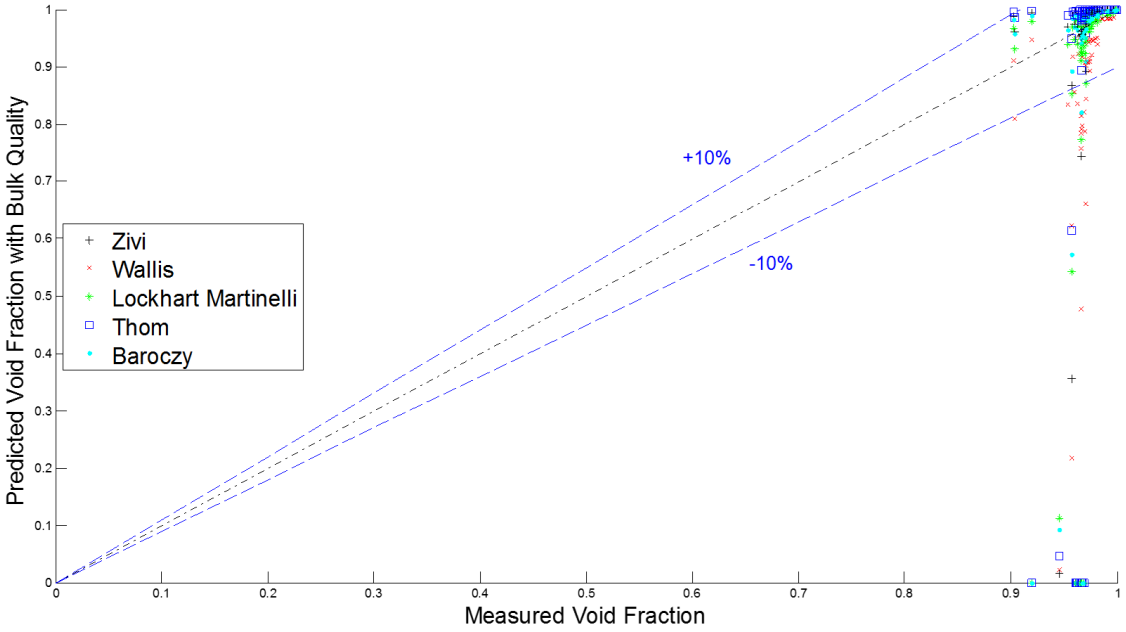

Figure 4-9 Comparison of Void Fraction Measurements to Predictions using Bulk Quality

Most recently, Xiao and Hrnjak [36] have taken the thermodynamic non-equilibrium phenomena into account for modeling heat transfer, void fraction and pressure drop in round tubes. The concept of superficial quality was proposed to resolve the inconsistency

in the non-equilibrium situation where a temperature gradient from vapor to the wall is physically evident as shown in Figure 4-10.

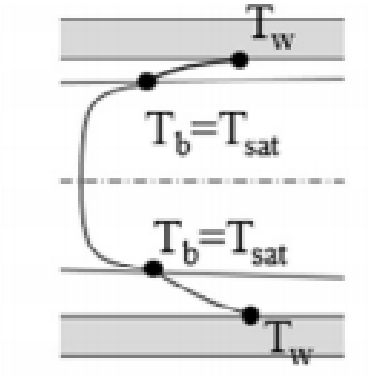

Figure 4-10 Temperature Profile in Condensing Two-Phase Flow (Used with permission from [36])

Instead of using saturation temperature to locate the end of condensation in traditional correlations, the bulk temperature which is defined as

$$T_b = T_{sat} - \frac{q''}{HTC} \tag{7}$$

was used to find the actual ending point of condensation. In Equation (7), q'' is the heat flux and HTC is the steam side heat transfer coefficient as if only condensate is flowing inside the tube. The corrected correlations of void fraction using superficial quality were plotted in Figure 4-11when inclination is 45°. Although not all measured points are on top of each curve, significant improvements were revealed for all correlations except Wallis'.

For all data points, comparisons between measured void fractions and predicted ones using superficial quality are shown in Figure 4-12. The same comparison was zoomed-in and plotted in Figure 4-13 to reflect the concentration of void fraction data near 0.95. Most of the corrected correlations can fit experimental data within ±10% except Wallis's.

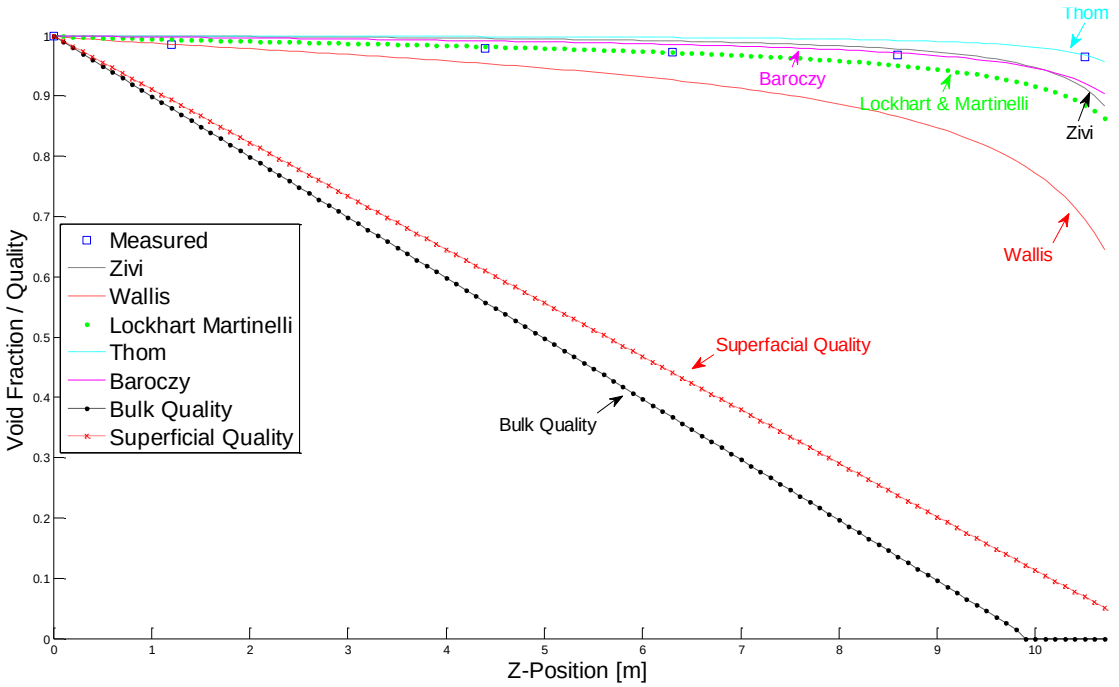

Figure 4-11 Void Fractions along the Tube at 45°: Measured vs Predicted by Superficial Quality

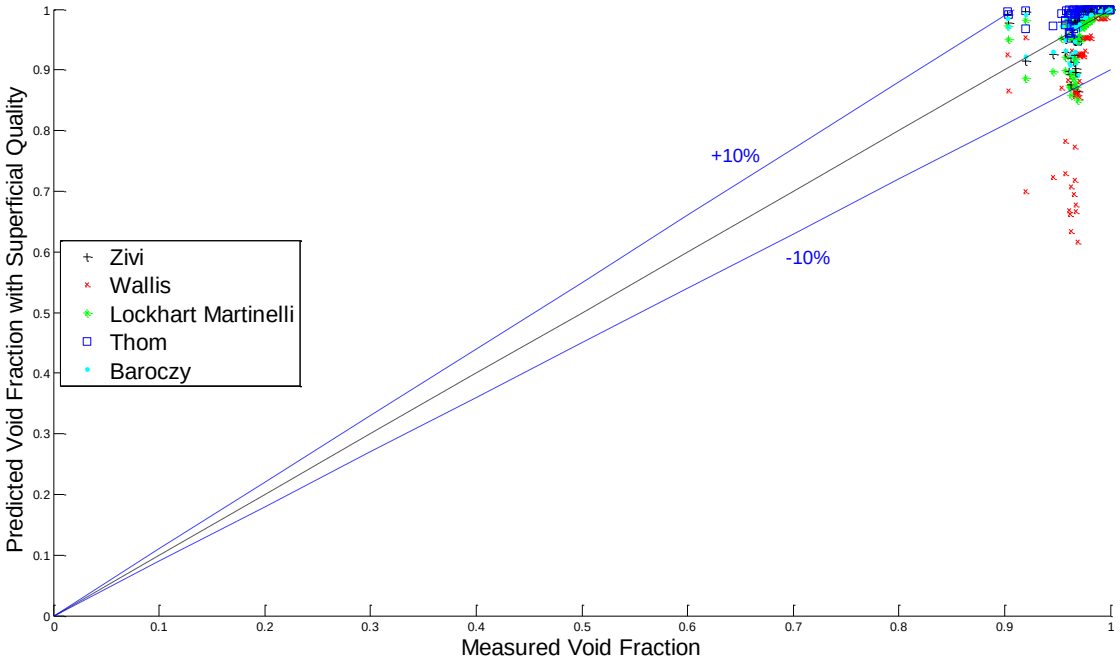

Figure 4-12 Comparison of Void Fraction Measurements to Predictions using Superficial Quality

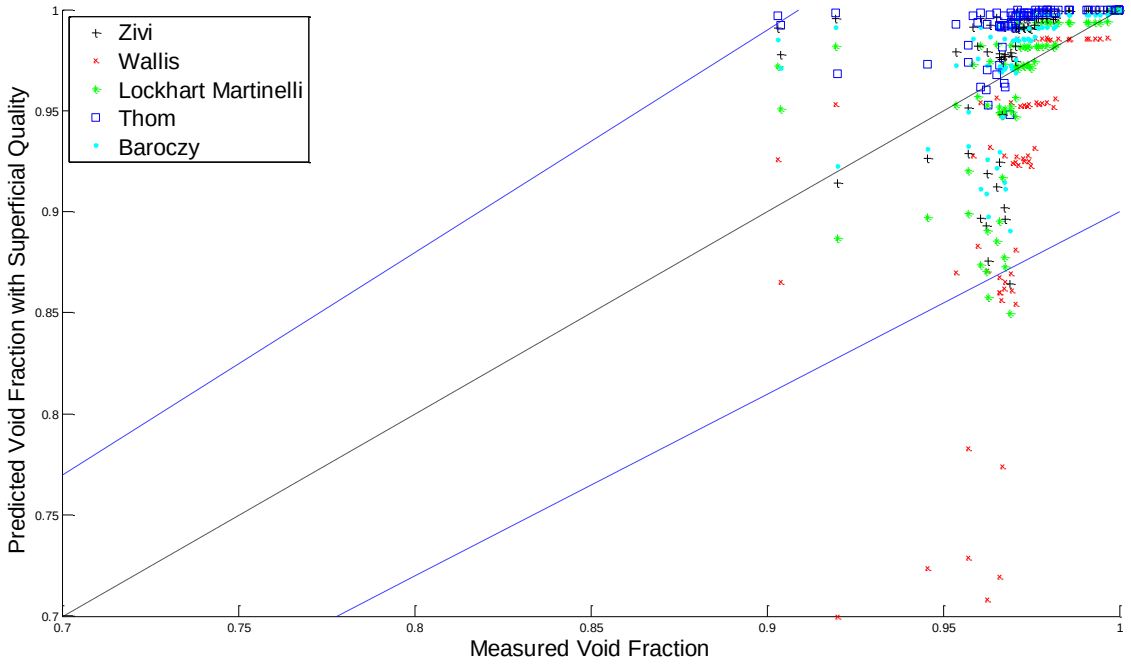

Figure 4-13 Comparison of Void Fraction Measurements to Predictions using Superficial Quality (Zoomed-In)

Although Lips and Meyer [27] found that the choice of void fraction correlations is not of great importance for determining momentum pressure drop, the apparent disagreement between measurement and predictions for void fraction in non-equilibrium conditions may lead to unexpected errors if the prediction of pressure drop involves void fraction correlations based on a thermodynamic equilibrium assumption. Therefore, a successful prediction using the corrected void fraction correlations would be very beneficial and was confirmed with the experimental data.

Chapter 5: Pressure Drop and Discussion

5.1 Conversion of Pressure Drop Measurements in Test Tube to Full Tube

The experiments were conducted in the half-size test tube for the purpose of visualization. However, such a design lost the capability of directly reflecting the effect of inclination angle on pressure drop for actual full-size air-cooled condensers in the power generation industry, so it is very essential to identify the differences between the test and full tube, and convert the experimental results to the results for the real geometry.

5.1.1 Differences in Tube Geometry and Flow Pattern

The creation of visualization access resulted in an artificial tube that was half-size compared to the original tube and was made of two distinct materials: steel and polycarbonate, as shown in Figure 3-4 (a) and Figure 3-5 (a). Such differences in geometry and material led to distinctive flow patterns during condensation in each type of tubes, as is illustrated in Figure 5-1, and thus complicated the process of directly comparing pressure drop in the actual, full-size condenser tubes in power plants to the experimental results from this facility. For instance, pressure drop inside the full tube came from the shears between liquid and steel wall, and between vapor and liquid interface; while the added adiabatic polycarbonate surface in the test tube maintained by the insulation created the additional shear between vapor and polycarbonate wall. Moreover, the smooth polycarbonate surface generated less frictional pressure drop than the rough steel surface, so it is essential to characterize the material surfaces in order to quantify the differences in pressure drops in these two types of tubes. Finally, the difference in cross-sectional area itself led to a difference in the area/volume ratio and therefore a difference in pressure drop. Therefore, a model to relate pressure drop in the test tube to the actual full size tube is needed in order to quantify the above-mentioned

differences. This model was proposed, elaborated and validated in the following sections throughout this chapter.

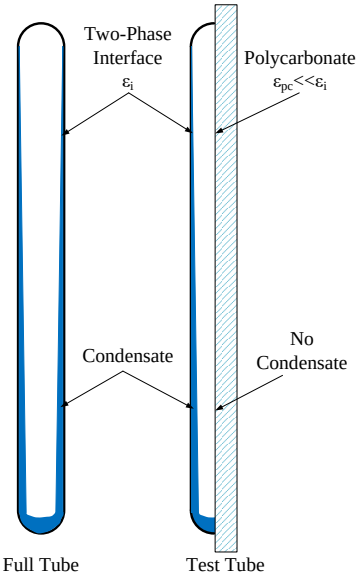

Figure 5-1 Different Flow Pattern in Full and Test Tubes

5.1.2 Surface Characterization and Modeling of Single Phase Pressure Drop

Consider a duct with arbitrary cross section area A and length L, the momentum equilibrium requires

$$A\Delta P_{fric} = \tau_w SL \tag{8}$$

where ΔP_{fric} is the frictional pressure drop across the duct, S is the perimeter of the duct cross section, and τ_w is the wall shear stress which is usually replaced by friction factor:

$$f = \frac{\tau_w}{1/2\,\rho V^2} \tag{9}$$

in which ρ is the fluid density, and V is the velocity of the flow. Applying the same analysis of pressure drop for the test tube, which was artificially made from steel and polycarbonate, the overall pressure drop of the fluid flowing across such tube should then

come from an overall wall shear stress, $\tau_{w,o}$, or equivalently an overall friction factor, f_o, which is from the shear between fluid and steel and the shear between the fluid and polycarbonate surface. The ratio of each individual contribution is proportional to the ratio of perimeter of each material in the tube to the total tube perimeter. Based on this fact, a simple linear model was proposed to quantify the effect of each individual contribution as

$$f_o = \omega_{st} f_{st} + (1-\omega_{st}) f_{pc} \tag{10}$$

where ω_{st} is the weight, or proportion, of steal side friction factor, f_{st}, on the overall friction factor, f_o, and f_{pc} is the polycarbonate side friction factor. The weights ω_{st} and $1-\omega_{st}$ are determined from test tube geometry measurement as

$$\omega_{st} = \frac{S_{st}}{S_{st} + H} \tag{11}$$

where S_{st} is the perimeter of steel in the cross section, and H is the height of the tube which is the same as the perimeter of polycarbonate in the cross section. In this study, $\omega_{st} = 0.5091$, and $1-\omega_{st} = 0.4909$.

In order to verify the validity of Equation (10), three independent experiments were conducted with single phase nitrogen gas running through a steel tube, polycarbonate duct, and the test tube. Note that the test tube, before cutting in half, was manufactured in the same batch as the full steel tube used in these single phase tests. From these three experiments, the surfaces of steel, polycarbonate and the composite surfaces in the test tube were characterized and then used to find f_{st}, f_{pc} and f_o. An additional overall

friction factor calculated from Equation (10) using measured f_{st} and f_{pc} were compared with the measured one so that the model could be checked and verified.

Figure 5-2 shows the single phase experiment in a full steel tube used for ACC systems in power plants. The tube geometry is highlighted in the same figure. The dots are the measured friction factors at different Reynolds number, and these data points were curve fitted by Churchill's [37], Colebrook's [38] and Haaland's [39] equations separately for obtaining the surface roughness of steel, ε_{st}. The Natarajan [40] model is shown for comparing its prediction for laminar rectangular duct flow only. Because of the goodness of the fit using Churchill's equation, ε_{st} was obtained to be 0.85 mm with a standard error of 0.07 mm. According to [41], a smooth steel tube usually has a roughness of about 0.05 mm, so such results indicated a slightly rusted steel surface internally, which was within expectations as the tube was not newly made. This surface roughness ε_{st} was then used to calculate f_{st} for other Reynolds numbers at other test conditions. The major sources of uncertainty in ε_{st} determination were from the low pressure drop measurements. At low Reynolds numbers, pressure drop was so small that the instrument limit was nearly reached. Even in the fully turbulent region when Re was above 7000, pressure drop was still below 100 Pa. This reasoning can be further supported by the measurement done in the polycarbonate duct in which the measurement points matched the predictions very well as shown in Figure 5-3.

Figure 5-3 is the friction factors measured in the polycarbonate duct that was made from the same polycarbonate used on the visualization window in the test tube. Experimental data aligned very well with the predictions by Colebrook for different small values of surface roughness and by Prandtl [42] for a smooth tube friction factor. As is expected

that the roughness of polycarbonate should be very small, the data validated the usage of the smooth tube assumption when predicting f_{pc} for different Reynolds numbers at other working conditions.

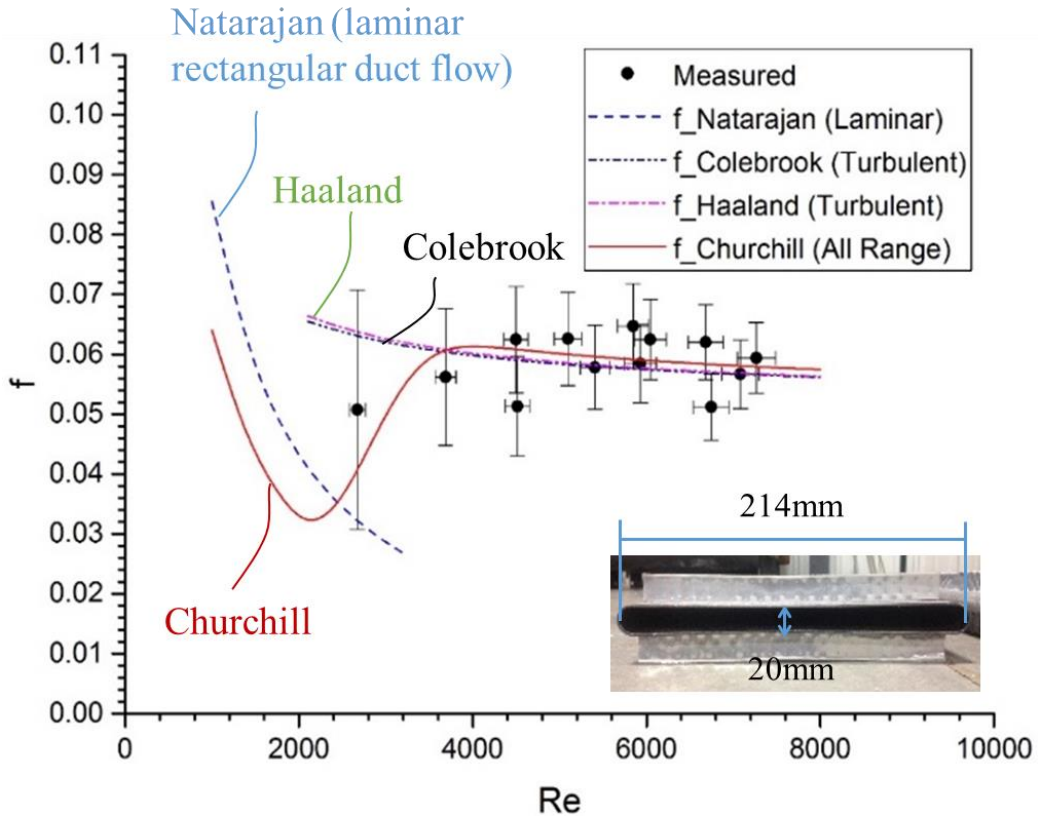

Figure 5-2 Steel Surface Characterization in Single Phase Test

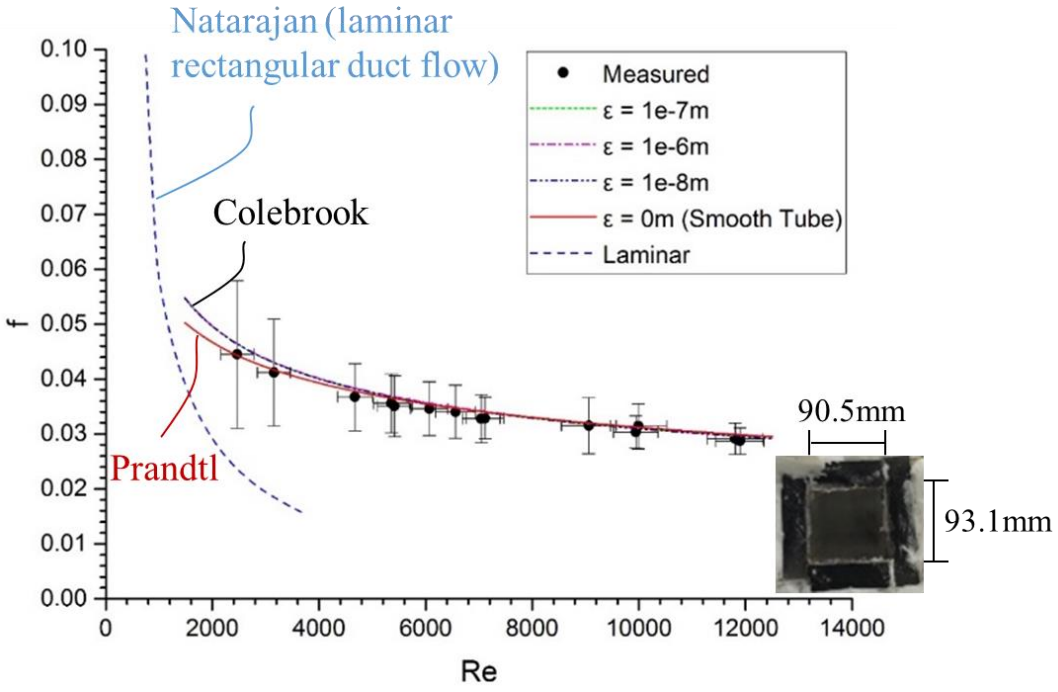

Figure 5-3 Polycarbonate Surface Characterization in Single Phase Test

Figure 5-4 shows the comparison between measured friction factor in the test tube to the predicted values from Equation (10) using the results from Figure 5-2 and Figure 5-3. The measured overall friction factors, $f_{o,m}$, are indicated as dots in the figure, and the predicted $f_{o,p}$ calculated from Colebrook's, Haaland's, and Churchill's equations using measured ε_{st} and ε_{pc} are shown as curves in the same figure. The predictions well agreed with the measurements within 5% in the transitional and turbulent region, and 40% in the laminar region. The large error in the laminar region mainly came from the uncertainty of small pressure drop measurements at low mass flow rate. Additionally, the Churchill equation works for predicting pressure drop in all ranges of Reynolds number, but it was originally developed based on the round tube measurements. So the difference between Natarajan's and Churchill's predictions shown in Figure 5-4 is justified, and experimental data fit Natarajan's correlation much better than Churchill's in the low Reynolds number region.

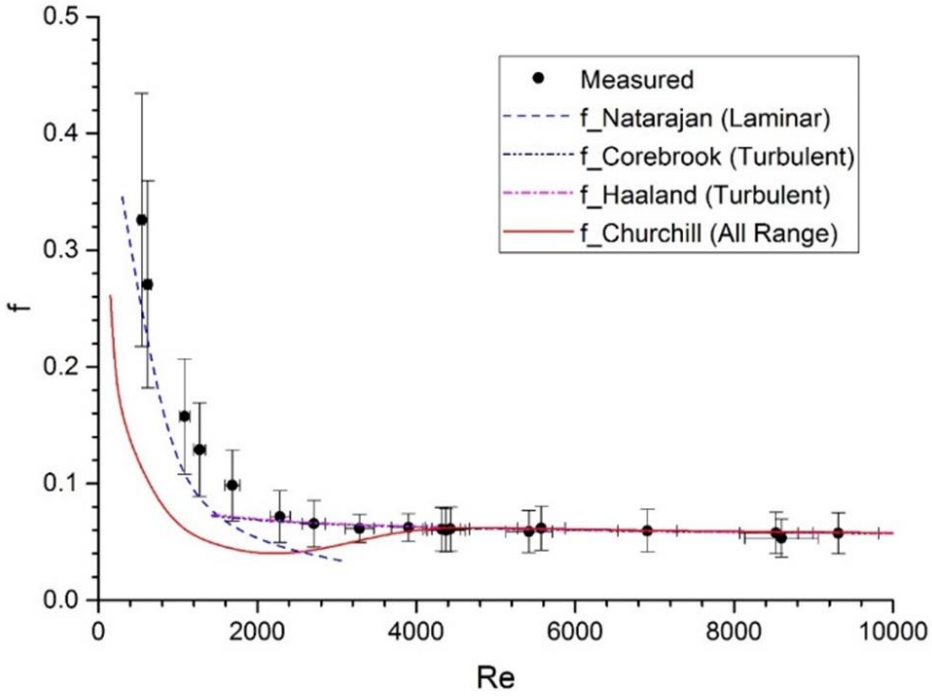

Figure 5-4 Comparison of Measured Friction Factor to Model Prediction

Overall, the model for quantifying the contribution of wall shears due to the composite surface material in the test tube was proven to be correct in the single phase test. The same logic can be applied to two phase experiments with some corrections specified for the two-phase situation in order to quantify the influences of different tube geometry and flow pattern in the test and full tube. With this useful tool that was elaborated in the next section, the experimental study in such a test tube can be directly translated into the results that would illustrate the pressure drop performance in the full-size actual condenser tubes in the ACC power plants.

5.1.3 Method of Relating Two-Phase Pressure Drops

Similar to Equation (10) in single phase, two-phase frictional pressure drop in the test tube $\Delta P_{fric,tt}$ across a finite tube length ΔL can be decomposed into two parts as

$$\left(\frac{\Delta P}{\Delta L}\right)_{fric,tt} = \left(\frac{\Delta P}{\Delta L}\right)_{i} + \left(\frac{\Delta P}{\Delta L}\right)_{pc} \tag{12}$$

where $\left(\frac{\Delta P}{\Delta L}\right)_i$ is the pressure drop per tube length due to the interfacial shear between vapor and liquid condensate, and $\left(\frac{\Delta P}{\Delta L}\right)_{pc}$ is the pressure drop per length due to the vapor shear on the polycarbonate wall. Based on the observed flow pattern that vapor and condensate liquid were well separated inside the tube, Equation (12) can be rewritten in the form similar to Taitel and Dukler's [8] stratified flow model as

$$-A_{g,tt}\left(\frac{dP}{dz}\right)_{fric,tt} - \tau_{pc}S_{pc} - \tau_{(i,w),tt}S_{(i,w),tt} - \tau_{(i,r),tt}S_{(i,r),tt} = 0 \qquad (13)$$

in which only frictional pressure drop was considered, $A_{g,tt}$ was derived from void fraction, and τ's and S's are the shears and perimeters of the corresponding components indicated by the subscripts in test tube as illustrated in Figure 5-5. Note that the liquid film on the steel wall was very thin and thus was neglected in determining $S_{(i,w),tt}$ and $S_{(i,r),tt}$.

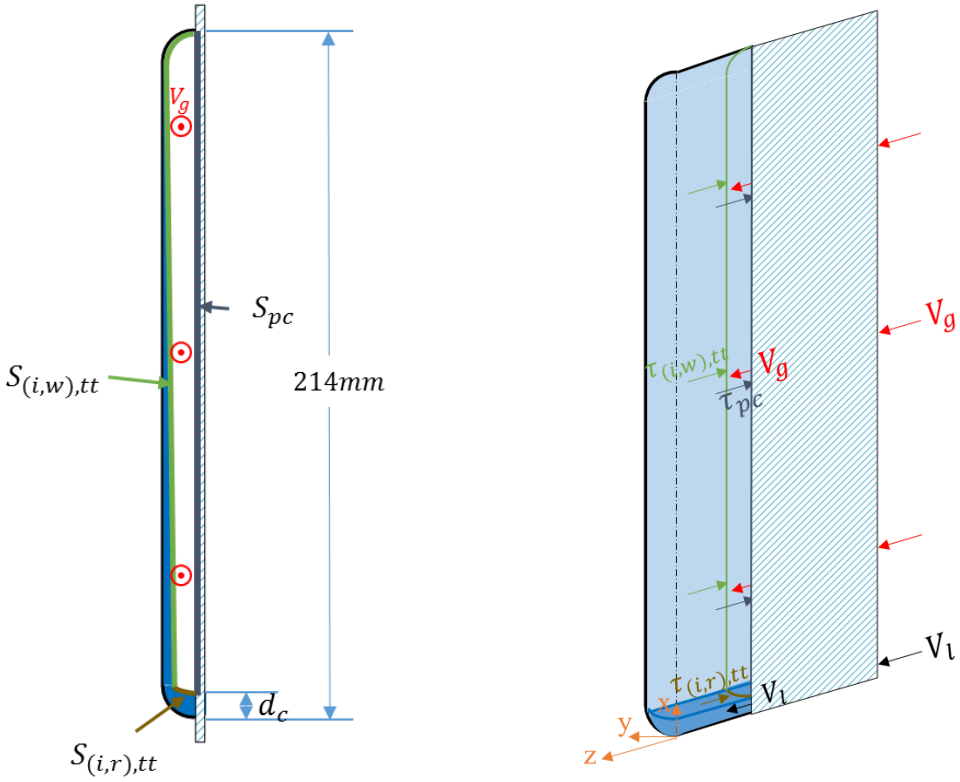

(a) (b)

Figure 5-5 Pressure Drop Components in the Test Tube: (a) 2D Cross-Sectional View, (b) 3D View

Similar to Equation (9), all the stresses in Equation (13) can be expressed as

$$\tau_{pc} = \frac{f_{pc}\rho_g V_g^2}{2} \tag{14}$$

$$\tau_{(i,w),tt} = \frac{f_{(i,w),tt}\rho_g V_g^2}{2} \tag{15}$$

$$\tau_{(i,r),tt} = \frac{f_{(i,r),tt}\rho_g (V_g - V_l)^2}{2} \tag{16}$$

where f_{pc} was determined using the smooth polycarbonate surface condition verified in the single phase test, $f_{(i,w),tt}$ was dependent on the interfacial surface roughness, ε_i,

between vapor and liquid film and droplets, and $f_{(i,r),tt}$ was calculated from Ouyang and Aziz's [10] correlation. Note that the velocity of the falling film was neglected and thus is not included in Equation (15).

The vapor shear on polycarbonate wall, τ_{pc}, occurred because of the special way of constructing the test tube, and hence is unique to the test tube. All the other shearing phenomena are common in both the test facility and the full condenser tube for ACC applications. So, similar to Equation (13) in test tube, the frictional pressure drop in a full tube can be written as

$$-A_{g,ft}\left(\frac{dP}{dz}\right)_{fric,ft} - \tau_{(i,w),ft}S_{(i,w),ft} - \tau_{(i,r),ft}S_{(i,r),ft} = 0 \tag{17}$$

where S 's were based on geometry of the full tube as illustrated in Figure 5-6, and τ's were obtained in the similar way as the shear stresses in the test tube except that the geometry differences need to be considered:

$$\tau_{(i,w),ft} = \frac{f_{(i,w),ft}\rho_g V_g^2}{2} \tag{18}$$

$$\tau_{(i,r),ft} = \frac{f_{(i,r),ft}\rho_g (V_g - V_l)^2}{2} \tag{19}$$

in which $f_{(i,w),ft}$ was calculated from the interfacial surface roughness, ε_i, for the flows in the full tube, and $f_{(i,r),ft}$ was obtained in the same method of $f_{(i,r),tt}$ after taking the tube size differences into account.

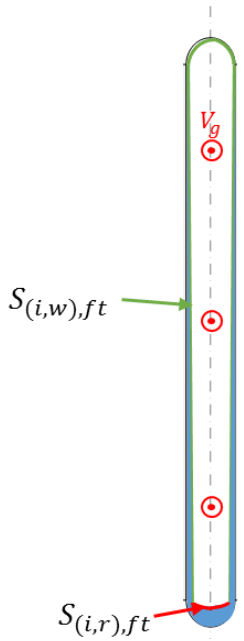

Figure 5-6 Illustration of Pressure Drop Components in the Full Tube

Fundamentally, the connection between the pressure drop in test tube and full tube is the interfacial roughness, ε_i, as friction factor was defined as a function of relative roughness, ε/D_h, and Reynolds number, Re, in commonly used correlations such as Haaland [39], Colebrook [38], Churchill [37] and so forth for the non-smooth tubes. As the tube size changes, both quantities would change.

Therefore, the actual conversion process started with the determination of the interfacial friction factor in the test tube, $f_{(i,w),tt}$, from Equation (13) through (16), as pressure drop was measured, geometry constants were known, and shear stresses on polycarbonate wall and condensate river were determined from velocity calculations and existing correlations for the friction factors. Then the interfacial surface roughness, ε_i, was calculated from $f_{(i,w),tt}$ using Haaland equation for turbulent vapor flow. After taking geometry difference into account, the same ε_i was used to get the interfacial friction factor in the full tube,

$f_{(i,w),ft}$, when vapor flow is turbulent, as the roughness only depends on material but not tube geometry. When vapor was laminar, frictional pressure drop was calculated from Natarajan's equation [40]. Finally the projected frictional pressure drops in the full tube, $\left(\frac{dP}{dz}\right)_{fric,ft}$, were able to be determined based on the full-tube pressure drop model descripted in Equation (17) through (19).

Noted that the above demonstrated conversion process is only for frictional pressure drop but not momentum and gravitational contributions in the total pressure drop. The determination of momentum and gravitational pressure are elaborated in Section 5.2.1 Data Reduction. Since the influences of different tube sizes in momentum and gravitational pressure drops are obvious and easy to be quantified, the total pressure drop in the full tube can be reasonably projected with such conversion process based on the measurements in the test tube. The final results are shown and discussed in Section 5.2.3 Converted Pressure Drop in Full-Size Tube.

5.2 Pressure Drop Measurements and Discussions

Raw pressure drop measurement data were collected under the conditions described in Table 3-1 and then processed. Under the same operating conditions, these processed pressure drop measurements in the test tube were further interpreted to show the pressure drops in full-size tube according to the method in the preceding section. Since actual ACC power plants almost always condense steam in the vacuum condition, the performance of pressure drops in vacuum were also predicted and discussed accordingly.

5.2.1 Data Reduction

Local pressure drops were recorded by five differential pressure transducers, and the overall pressure drop from inlet to outlet can then be derived by adding all five local

pressure drops together. In addition, two pressure sensors measuring gauge pressures at inlet and outlet independently collected overall pressure drop that was obtained by subtracting outlet gauge pressure from the inlet. Having independent and redundant measurements, the actual overall pressure drop can then be combined reasonably based on the approach suggested by Park et al [43] aiming to minimize combined experimental uncertainty. The local pressure drops were scaled accordingly to match the combined overall pressure drop. Details about this uncertainty-analysis aided approach are discussed in Appendix A: Uncertainty Analysis. Denote local and overall combined pressure drop after this first step as $\Delta P_{com,j}$ where $j = 1, 2, ..., 5$ and $\Delta P_{com,o}$, respectively.

The actual pressure drops ΔP's in the tube can be deduced from the combined pressure drops ΔP_{com}'s, and the corrections ΔP_{hose}'s as:

$$\Delta P_{test,j} = \Delta P_{com,j} - \Delta P_{hose,j} \tag{20}$$

where $j = 1, 2, ..., 5$ represents local information and $j = o$ refers to overall, and ΔP_{hose} were originated from the hydrostatic pressure difference in the hoses connecting measurement port to pressure sensor.

As the steam condensation in the test tube was carried out at pressures slightly higher than atmospheric pressure, the system was not vacuumed before condensing the steam and air was trapped inside the pressure measurement hose throughout the entire process. The positive internal pressure of the test tube with respect to atmospheric pressure guaranteed that air was not leaked into the condenser to degrade the heat transfer. Due to this positive pressure, small amounts of steam could flow into the hoses and then condense because of the lower ambient temperature at the beginning of experiments, but this process did not last long as the volume of air in the pressure hose decreased due to

the incoming condensate and finally the pressure of air in the pressure measurement hoses balanced with the internal pressure. So the correction of pressure drop in the connecting hoses can be quantified as

$$\Delta P_{hose} = \rho_a g \Delta L \sin\varphi \tag{21}$$

For two-phase flows, the measured pressure drops, ΔP_{tot}, are the sum of three contributions: the frictional pressure drop, ΔP_{fric}, the momentum pressure drop, ΔP_{mom}, and gravitational pressure drop, ΔP_{grav}:

$$\Delta P_{tot} = \Delta P_{fric} + \Delta P_{mom} + \Delta P_{grav} \tag{22}$$

For inclined downward flow, the gravitation pressure drops are negative and depend on inclination angle:

$$\Delta P_{grav} = -\left[\rho_l (1-\alpha) + \rho_v \alpha\right] g \Delta L \sin\varphi \tag{23}$$

The momentum pressure drop is also referred to as acceleration pressure drop for flow in boiling and deceleration pressure drop for flow in condensation. Its magnitude reflects the amount of changes in kinetic energy of the flow to pressure losses or gains for boiling and condensation respectively, and is determined as

$$\Delta P_{mom} = G^2 \left[\left(\frac{(1-x)^2}{\rho_l (1-\alpha)} + \frac{x^2}{\rho_v \alpha} \right)_{out} - \left(\frac{(1-x)^2}{\rho_l (1-\alpha)} + \frac{x^2}{\rho_v \alpha} \right)_{in} \right] \tag{24}$$

where the subscripts in and out refer to the inlet and outlet of each measurement section. For condensation, momentum pressure drop is also always negative, meaning that pressure is recovered as vapor condenses along the tube.

Rearranging Equation (22), frictional pressure drop can be obtained after evaluating

gravitational and momentum pressure drop in Equation (23) and (24) as:

$$\Delta P_{fric} = \Delta P_{tot} - \Delta P_{mom} - \Delta P_{grav} \tag{25}$$

5.2.2 Pressure Drop Analysis in Test Tube

The overall pressure drops of steam condensation in the 10.7 m long test tube measured at various inclination angles were plotted in Figure 5-7, in which the linear trend lines are also shown for each component. The test conditions such as mass flux of steam and ambient temperatures were also labeled in the same figure. Despite the fact that mass flux and ambient temperatures were very difficult to control because of the complexity and the large scale of the system, their variations were found to be within 10%. The experimental data showed a clear trend of negative dependence of pressure drop on inclination angle.

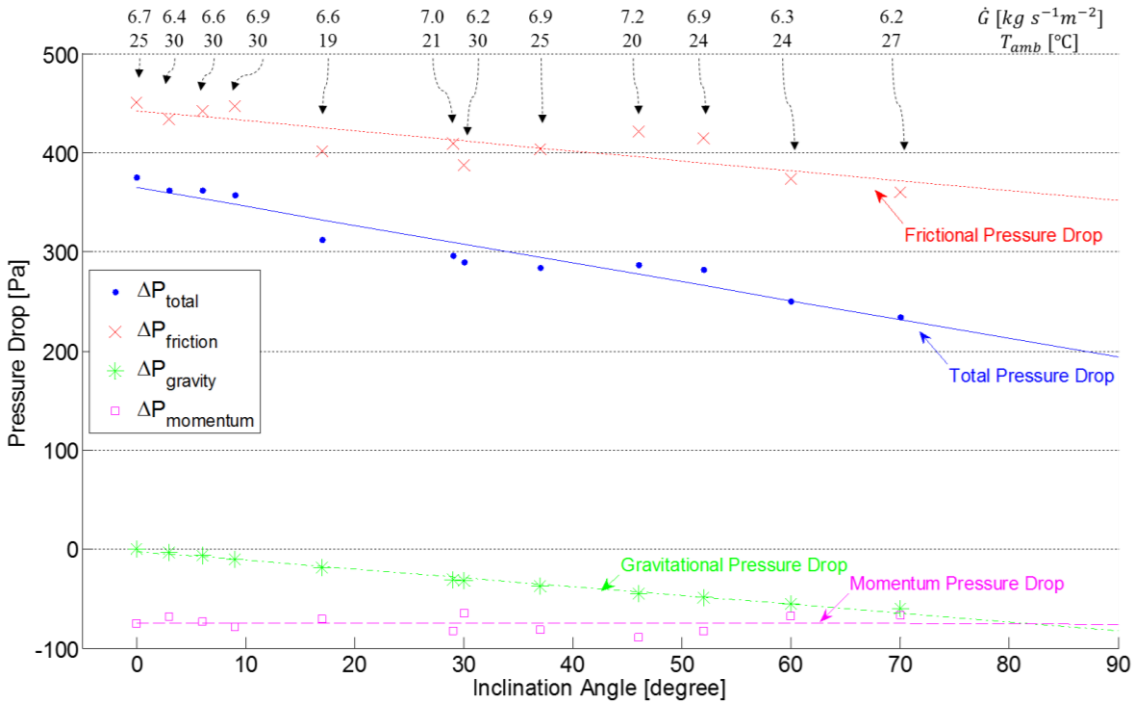

Figure 5-7 Overall Pressure Drop at Different Inclination Angles in Test Tube

The total pressure drop in this study, which included all three pressure-drop contributions,

decreased as inclination angle increased. This can be explained by several facts: firstly, the gravitational pressure drop decreased almost linearly with inclination angle. In this downward flow configuration, gravity helped to recover the pressure and decrease the total pressure drop; secondly, higher inclination angles increased void fraction throughout the entire tube, as seen in Figure 4-7. The increased void fraction slowed down the vapor velocity, caused less shear between phases and finally lowered the frictional pressure losses and thus total pressure drop; lastly, the momentum pressure drop was found to be almost unaffected by inclination angles, and did not affect too much the trend of total pressure drop. Similar to the results reported by O'Donovan and Grimes [31], the total pressure drops were found to be quite small. However, their reported frictional pressure drop and momentum recovery were comparably larger than the ones in this study mainly because they had much higher vapor velocities under the vacuum operating condition.

After removing out the gravitational and momentum pressure drop from the total pressure drop, the local and overall frictional pressure drops as a function of inclination angles were plotted in Figure 5-8, in which the illustration on the left shows the relative location of each local pressure drop measurement section with respect to the steam flow direction.

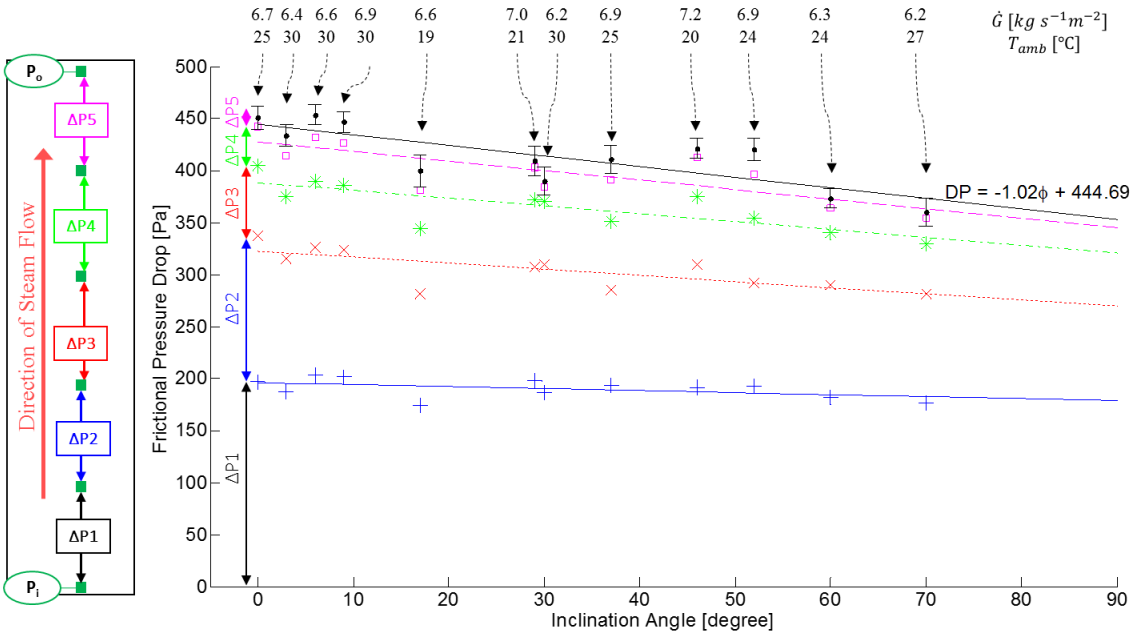

Figure 5-8 Local and Overall Frictional Pressure Drop in the Test Tube

As can be seen in Figure 5-8, local frictional pressure drops that were described by the vertical distance between each adjacent trend lines, ΔP_1 to ΔP_5, decreased along the steam flow direction due to the deceleration of vapor. Also, these local pressure drops decreased when the tube was tilted more and more in the downward direction. At higher inclination angle, the velocity difference between vapor and liquid became smaller as liquid was accelerated by gravity and vapor was decelerated more due to the increased void fraction. Therefore, the interfacial shear was decreased, and so were the frictional pressure drops. Although not all the data points were on the trend lines because of the slight differences in operating conditions, the trend is still very clear and strong.

The frictional pressure drops in the test tube were originated from interfacial shear between vapor and condensate as well as between vapor and polycarbonate wall, which have been characterized in detail in Figure 5-5. One of the fundamental parameters for quantifying the frictional loss in an internal flow is the surface roughness, which also

serves as a link to relate pressure drop between the friction in the test tube and full tube under the same operating conditions. However, in the two-phase flow, such roughness is not usually defined as a function of tube material but is characterized by the interfacial behaviors of the two phases. Following the steps described in Section 5.1.3, the interfacial surface roughness, ε_i, was determined and is shown in Figure 5-9.

The magnitude of interfacial surface roughness in Figure 5-9 tended to increase towards the end of the tube, but the uncertainty associated with such increasing trend also enlarged significantly due to the low Reynolds number of vapor flow. As has been indicated in the same figure, the vapor flowed in transition or laminar regions at about 7 m away from tube inlet. With low vapor velocity near the exit, the influence of surface roughness in frictional pressure drop became negligible especially when flow was in laminar region in which friction factor did not depend on roughness any more. Therefore, although a large deviation of interfacial roughness was found at low Reynolds number, the uncertainty of frictional pressure drop in the same region was almost unaffected. Furthermore, no obvious dependence of roughness on inclination angle was discovered, which implied that the changes in inclination didn't affect the interfacial behavior too much. Instead, higher inclination angles increased void fraction, reduced vapor velocity, and finally decreased the frictional pressure drop. Finally, the magnitude of the obtained interfacial roughness in the fully turbulent region (close to the inlet) was about 0.3 mm. Given the facts that smooth steel tube usually has a surface roughness about 0.05 mm [41] and the roughness of the steel tube in this study was measured to be 0.8 mm in Section 5.1.2, the condensate on the tube wall helped smoothen the original tube surface but kept it rougher than the smooth steel. This could be true because mass flux of steam was very low compared to usual refrigeration system, where mass flux is typically over 50 kg m^{-2} s^{-1} and strong interaction of vapor and liquid significantly roughens the interface and thus

leads to an interfacial roughness that is higher than the roughness of the tube surface.

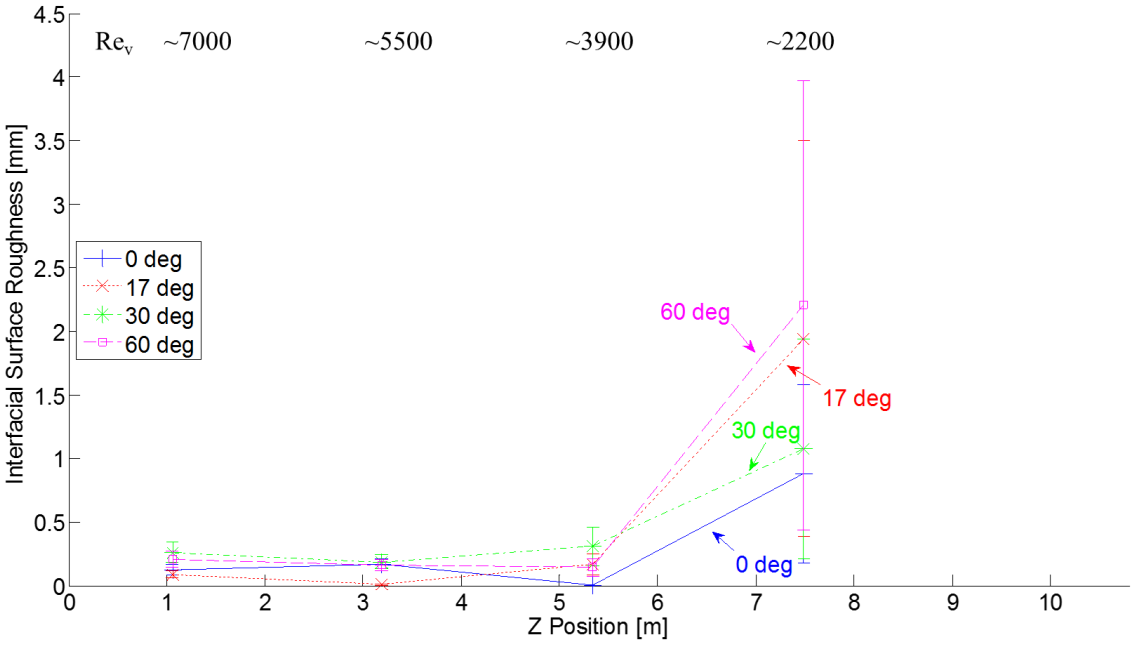

Figure 5-9 Interfacial Surface Roughness along the Test Tube at Various Inclination Angles

5.2.3 Converted Pressure Drop in Full-Size Tube

Heat flux and mass flux were kept the same in both test tube and full tube, so identical vapor and liquid velocities, void fractions and quality variations along the tubes were expected in the two systems. The difference in tube cross-section geometry affected the magnitude of Reynolds number, and thus friction factor and frictional pressure drop, but the fundamental quantity of interfacial roughness was unchanged with tube size. Having the pressure drop data and results in test tube available, the conversion for pressure drop in full tube under the above mentioned conditions was determined, following the approach described in Section 5.1.3., and plotted in Figure 5-10 and Figure 5-11.

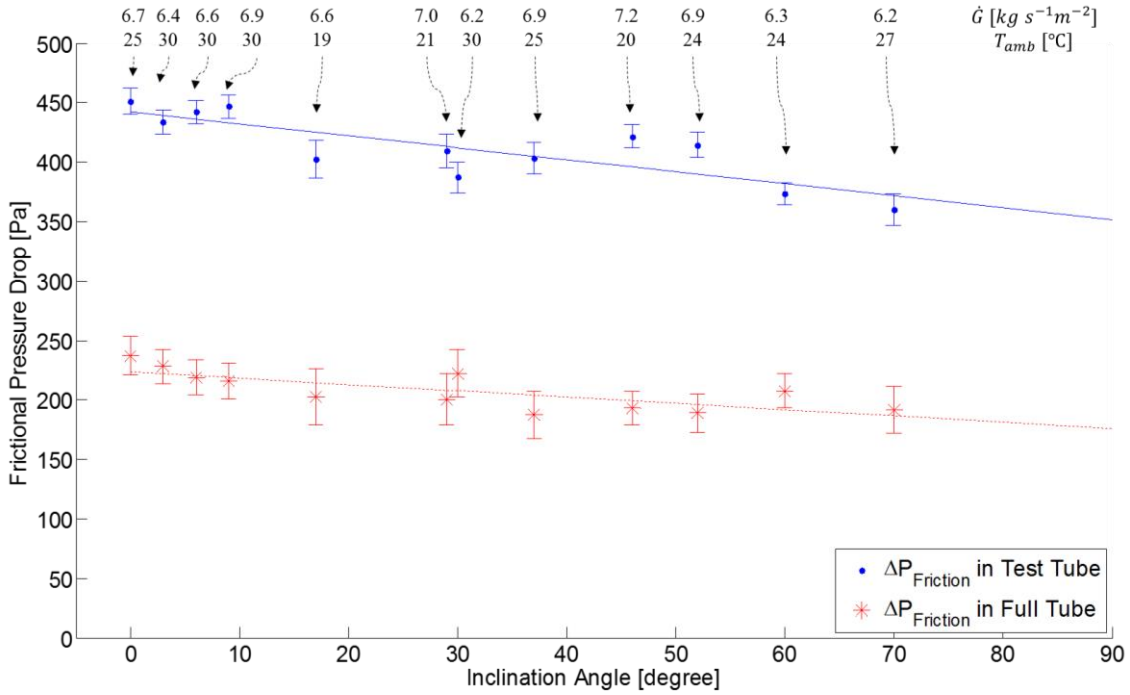

Figure 5-10 Comparison of Frictional Pressure Drops in Test and Full Tubes

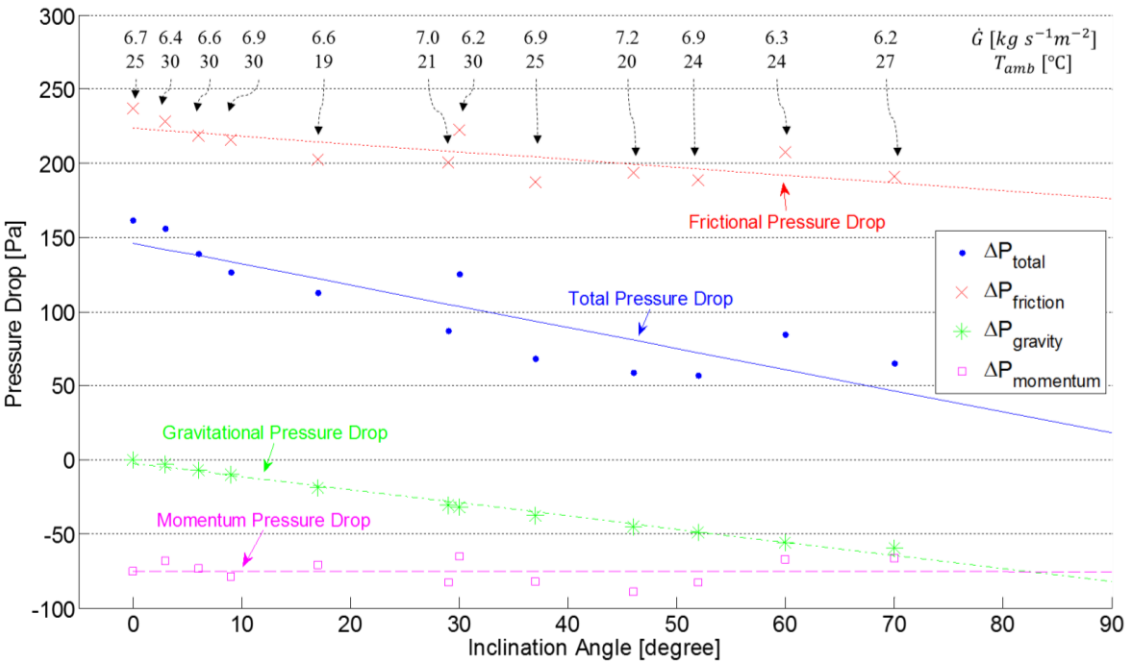

Figure 5-11 Converted Pressure Drops in Full Tube

Figure 5-10 compares the frictional pressure drop in test and full tubes. As the cross-sectional area enlarged in the full tube, the same vapor velocities led to larger Reynolds

number but lower friction factor. So lower frictional pressure drop in the full tube was expected and discovered. The decreasing trend of frictional pressure drop over inclination angle was also captured in the full tube, but the dependence was not as strong as it was in the test tube. This phenomenon can be explained by invoking the fundamental equation for determining frictional pressure drop for internal flow:

$$\Delta P_{fric} = f \frac{L}{D} \frac{1}{2} \rho V^2 \tag{26}$$

Firstly, surface roughness had no strong dependence on inclination angle as shown in Figure 5-9, so neither did friction factor. So the decrement in pressure drop at higher inclination angle was not strongly affected by the friction factor, f. Secondly, as was discussed that the slower vapor velocity at higher inclination angles due to larger void fractions was the dominating factor that lowered pressure drop in the test tube, the same conclusion can be drawn in the full tube. However, because of the larger cross sectional area, increased hydraulic diameter in the denominator of Equation (26) weakened the decreasing trend in velocity. Therefore, although the frictional pressure drop in the full tube also decreased as inclination became higher, the slope was less steep compared to that for the smaller test tube.

Similar to Figure 5-7, the total pressure drop in full tube comprised frictional, momentum and gravitational pressure drops. The overall pressure drop from tube inlet to outlet decreased at higher inclination angle as plotted in Figure 5-11. Under the same conditions, the magnitudes of momentum and gravitational pressure drops were the same in full tube as those in test tube and were also negative. Due to the fact that frictional loss in full tube was less than it was in test tube, the overall pressure drop could become very small and close to zero. The low pressure drops at high inclination angles indicated that the system pressure can be recovered by the momentum loss and gravity, and thus implied that

natural gravitational force would be very helpful for driving the vapor flow in the tube and no or little external pumping power is indeed needed. However, this is only true if the system runs at the same condition as it was in the test tube. In reality, the ACC power plants are operating in vacuum condition, and thus the gravitational recovery becomes negligible as vapor density is very small. Also, the frictional loss and momentum recovery would increase dramatically due to the very high vapor velocity as have been discussed in [31].

5.2.4 Predicted Pressure Drops under Vacuum Operating Conditions

Due to the difference in operating conditions between actual ACC system in power plants and the test system in this study, it is inappropriate to draw a conclusion that the discoveries in this study are directly applicable to the real systems. Thus a further analysis of the experiment results was carried out to predict the pressure drop performance in the real ACC system under vacuum condition.

When steam is condensed in vacuum at the same mass flux, its velocity would increase significantly due to the decrease in density at low pressure. Intuitively, heat transfer coefficient on the steam side would also increase and thus lead to lower qualities and void fractions at the same location in the condenser tube compared to the ones at atmospheric pressure in this study. Due to the limited number of research on ACC systems with large flattened tubes in the open literature, there are no appropriate numerical models available to exactly predict heat transfer without conducting actual experiments. So the prediction had to be done by assuming that the quality and void fraction variations are the same in the vacuum condition and the condition used in this study. However, such assumptions are not unrealistic because the air side heat transfer can always be controlled in a real system in order to match the conditions imposed by the identical heat transfer rate requirement. Nonetheless, such a prediction is able to provide a qualitative foresight of

the dependence of pressure drop on inclination angle in real operating conditions. Referring to the overview [44], the operating temperature of the steam condenser in ACC power plants varies between 60 ^{o}C to 80 ^{o}C. Aiming to be closer to reality, the predicted pressure drop was plotted in Figure 5-12 when steam saturation temperature is 60^{o}C.

As is expected, the magnitude of frictional loss and momentum recovery increased significantly while gravitational pressure drop became negligible due to the low vapor density and high vapor velocities compared to the ones under atmospheric condition as shown in Figure 5-7 and Figure 5-11. The total pressure drop also increased as a result of higher frictional loss. Most importantly, the same trend of pressure drop on inclination angle was found that higher inclination decreases the frictional and total pressure drops in the vacuum condition. Therefore, by changing the condenser tube inclination, better performance can be achieved in the ACC system in terms of pressure drop reduction.

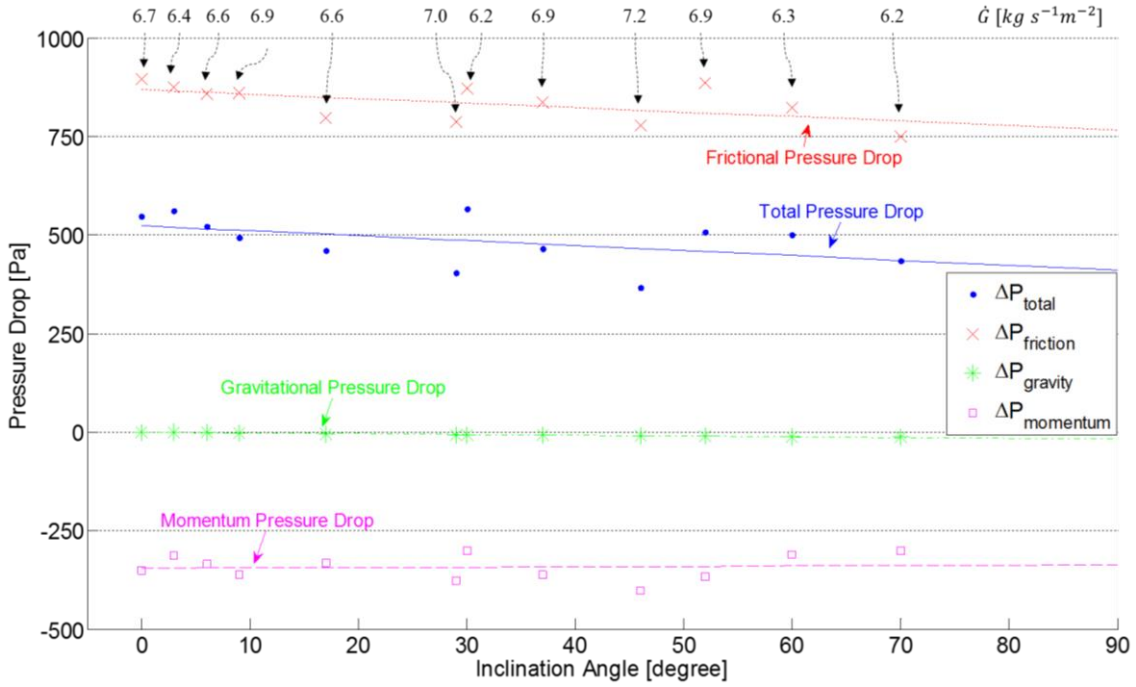

Figure 5-12 Predicted Pressure Drop in Full Tube under Vacuum Operating Condition

Chapter 6: Conclusions

Flow regimes were observed for all inclination angles from 0 to 70^{o}. The results showed that a mixed mode of film and dropwise condensation of steam occurred on the steel tube wall, and slid down to the condensate river on the bottom of the tube. The river depth increased along the tube at all inclination angles except at horizontal as gravity dominated the condensate flow at inclined conditions but not at horizontal. At the same location, the depth decreased at higher inclination angle due to the gravity-assisted drainage. The measurements of condensate river depth enabled the evaluation of void fractions, and a successful prediction of void fractions in the thermodynamic non-equilibrium condition was provided using the superficial quality from Xiao and Hrnjak [36].

Two-phase pressure drop was measured in the test system, and the results showed the overall pressure losses were relatively small, in the range of 200 to 400 Pa. Based on visualizations that the flow pattern was separated for all downward inclination angles, a pressure drop model was developed to characterize the contributions of each surface inside the tube. This model was implemented to convert pressure drop measurements in the test tube to predicted pressure drop in the full tube under the same operating conditions, and to predict the pressure drop in vacuum keeping heat transfer rate the same. Both measurements and the predictions in atmospheric pressure and vacuum showed the decreasing trend of in-tube pressure drop as inclination angle increased. Such a trend was consistent with the visualization results that gravity played the major role in enlarging void fraction and slowing down the vapor velocity at higher inclination angles. Due to the lack of relevant research on inclined condensation, particularly with a flattened tube, the exact magnitudes of predicted results were not able to be verified quantitatively. However, the strong dependence of pressure drop on inclination angle was discovered and confirmed from both the measurements and visualization.

References

[1] A. E. Conradie and D. G. Kröger, "Performance Evaluation of Dry-Cooling Systems for Power Plant Application," *Applied Thermal Engineering*, pp. 219-232, 1996.

[2] M. Maupin, J. Kenny, S. Hutson, J. Lovelace, N. Barber and K. Linsey, "Estimated Use of Water in the United States in 2010," U.S. Geological Survey Circular 1405, 2014.

[3] E. Shuster, "Estimating Freshwater Needs to Meet Future Thermoelectric Generation Requirements," National Energy Technology Laboratory, 2007.

[4] R. W. Lockhart and R. C. Martinelli, "Proposed Correlation of Data for Isothermal Two-Phase Two-Component Flow in Pipes," *Chemical Engineering Progress*, vol. 45, no. 1, pp. 39-48, 1949.

[5] D. Chisholm and A. D. K. Laird, "Two-Phase Flow in Rough Tubes," *Trans. ASME*, vol. 80, pp. 276-286, 1958.

[6] L. Friedel, "Improved Friction Pressure Drop Correlations for Horizontal and Vertical Two-Phase Pipe Flow," in *European Two Phase Flow Group Meeting*, Ispra, Italy, 1979.

[7] V. P. Carey, Liquid-Vapor Phase-Chamge Phenomena, New York: Taylor & Francis Group, LLC, 2008.

[8] Y. Taitel and A. E. Dukler, "A Model for Predicting Flow Regime Transitions in Horizontal and Near Horizontal Gas-Liquid Flow," *AlChE Journal*, vol. 22, no. 1, pp. 47-55, 1976.

[9] J. E. Kowalski, "Wall and Interfacial Shear Stress in Stratified Flow in a Horizontal Pipe," *AIChE Journal*, vol. 33, no. 2, pp. 274-281, 1987.

[10] L. Ouyang and K. Aziz, "Development of New Wall Friction Factor and Interfacial Friction Factor Correlations for Gas-Liquid Stratified Flow in Wells and Pipelines," in *Society of Petroleum Engineers Western Regional Meeting*, Anchorage, Alaska, 1996.

[11] G. B. Wallis, One-dimensional Two-phase Flow, McGraw-Hill, Inc, 1969.

[12] J. G. Collier, Convective Boiling and Condensation, McGraw-Hill, 1972.

[13] M. Sadatomi and Y. Sato, "Two-Phase Flow in Vertical Noncircular Channels," *International Journal of Multiphase Flow*, vol. 8, no. 6, pp. 641-655, 1982.

[14] H. Ide and H. Matsumura, "Frictional Pressure Drops of Two-Phase Gas-Liquid

Flow in Rectangular Channels," *Experimental Thermal and Fluid Science,* pp. 362-372, 1990.

[15] K. Akagawa, "The Flow of Mixture of Air and Water: the Friction Losses in Horizontal, Inclined and Vertical Tubes," *Trans. JSME,* vol. 23, no. 128, p. 292, 1957.

[16] M. W. Wambsganss, J. A. Jendrzejczyk, D. M. France and N. T. Obot, "Frictional Pressure Gradients in Two-Phase Flow in a Small Horizontal Rectangular Channel," *Experimental Thermal and Fluid Science,* pp. 40-56, 1992.

[17] H. J. Lee and S. Y. Lee, "Pressure Drop Correlations for Two-Phase Flow Within Horizontal Rectangular Channels with Small Heights," *International Journal of Multiphase Flow,* pp. 783-796, 2001.

[18] K. Mishima, T. Hibiki and H. Nishihara, "Some Characteristics of Gas-Liquid Flow in Narrow Rectangular Ducts," *International Journal of Multiphase Flow,* vol. 19, no. 1, pp. 115-124, 1993.

[19] J. W. Coleman and S. Garimella, "Two-Phase Flow Regimes in Round, Square and Rectangular Tubes during Condensation of Refrigerant R134a," *International Journal of Refrigeration,* pp. 117-128, 2003.

[20] M. J. Wilson, T. A. Newell, J. C. Chato and C. A. Infante Ferreira, "Refrigerant Charge, Pressure Drop, and Condensation Heat Transfer in Flattened Tubes," *International Journal of Refrigeration,* vol. 26, pp. 442-451, 2003.

[21] D. S. Jung and R. Radermacher, "Prediction of Pressure Drop during Horizontal Annular Flow Boiling of Pure and Mixed Refrigerants," *Internaltional Journal of Heat Transfer,* vol. 32, no. 12, pp. 2435-2446, 1989.

[22] N. H. Kim, E. J. Lee and H. W. Byun, "Condensation Heat Transfer and Pressure Drop in Flattened Smooth Tubes Having Different Aspect Ratios," *Experimental Thermal and Fluid Science,* vol. 46, pp. 245-253, 2013.

[23] H. Muller-Steinhagen and K. Heck, "A Simple Friction Pressure Drop Correlation for Two-Phase Flow in Pipes," *Chem. Eng. Processing,* vol. 20, pp. 297-308, 1986.

[24] S. Lips and J. P. Meyer, "Two-Phase Flow in Inclined Tubes with Specific Reference to Condensation: A Review," *International Journal of Multiphase Flow,* vol. 37, pp. 845-859, 2011.

[25] H. D. Beggs and J. P. Brill, "A Study of Two-Phase Flow in Inclined Pipes," *Journal of Petroleum Technology,* vol. 25, pp. 607-617, 1973.

[26] P. Andreussi and L. N. Persen, "Stratified Gas-Liquid Flow in Downwardly Inclined Pipes," *International Journal of Multiphase Flow,* vol. 13, no. 4, pp. 565-575, 1987.

[27] S. Lips and J. P. Meyer, "Experimental Study of Convective Condensation in an Inclined Smooth Tube. Part II: Inclination Effect on Pressure Drops and Void Fractions," *International Journal of Heat and Mass Transfer,* vol. 55, pp. 405-412, 2012.

[28] A. O. Adelaja, J. Dirker and J. P. Meyer, "Experimental Study of the Pressure Drop during Condensation in an Inclined Smooth Tube at Different Saturation Temperatures," *International Journal of Heat and Mass Transfer,* vol. 105, pp. 237-251, 2017.

[29] D. G. Kröger, "Air-Cooled Heat Exchangers and Cooling Towers: Thermal-Flow Performance Evaluation and Design," Oklahoma, PennWell, 2004, p. 336.

[30] A. O'Donovan and R. Grimes, "A Theoretical and Experimental Investigation into the Thermodynamic Performance of a 50 MW Power Plant with a Novel Modular Air-Cooled Condenser," *Applied Thermal Engineering,* vol. 71, pp. 119-129, 2014.

[31] A. O'Donovan and R. Grimes, "Pressure Drop Analysis of Steam Condensation in Air-Cooled Circular Tube Bundles," *Applied Thermal Engineering,* vol. 87, pp. 106-116, 2015.

[32] W. A. Davies, "Heat Transfer and Visualization in Large Flattened-Tube Condensers with Variable Inclination (Master Thesis)," University of Illinois at Urbana-Champaign, 2016.

[33] J. R. S. Thom, "Prediction of Pressure Drop during Forced Circulation Boiling of Water," *International Journal of Heat and Mass Transfer,* vol. 7, pp. 709-724, 1964.

[34] C. J. Baroczy, "Correlation of Liquid Fraction in Two-Phase Flow with Applications to Liquid Metals," *Chemical Engineering Progress Symposium Series,* vol. 61, no. 57, pp. 179-191, 1965.

[35] S. M. Zivi, "Estimation of Steady-State Steam Void-Fraction by Means of the Principal of Minimum Entropy Production," *Journal of Heat Transfer,* vol. 86, pp. 247-252, 1964.

[36] J. Xiao and P. Hrnjak, "Heat Transfer and Pressure Drop of Condensation From Superheated Vapor to Subcooled Liquid," *International Journal of Heat and Mass Transfer,* vol. 103, pp. 1327-1334, 2016.

[37] S. Churchill, "Friction factor equation spans all fluid flow regimes," *Chemical Engineering,* pp. 91-92, 1977.

[38] C. Colebrook and C. White, "Experiments with fluid friction in roughened pipes," *Proceedings of the Royal Society of London. Series A, Mathematical and Physical Sciences* , pp. 367-381, 1937.

[39] S. Haaland, "Simple and explicit formulas for the friction factor in turbulent pipe flow," *Journal of Fluids Engineering*, pp. 89-90, 1983.

[40] N. Natarajan and S. Lakshmanan, "Laminar flow in rectangular ducts: Prediction of velocity profiles and friction factor," *Indian Journal of Science and Technology*, 1972.

[41] A. F. Mills and V. Ganesan, "Rough Surfaces," in *Heat Transfer*, Pearson, 2013, p. 137.

[42] L. Prandtl, Essentials of Fluid Dynamics, London: Blackie & Son, 1969.

[43] Y.-G. Park, L. Liu and A. M. Jacobi, "Rational Approaches for Combining Redundant, Independent Measurements to Minimize Combined Experimental Uncertainty," *Experimental Thermal and Fluid Science*, vol. 34, pp. 720-724, 2010.

[44] J. Shi, "World's Largest Power Plant Dry Cooling Systems Overview," in *EPRI Brown Bag Lunch Seminar*, Palo Alto, CA, 2013.

Appendix A: Uncertainty Analysis

A.1 Measurement Uncertainty

Temperatures, pressure and mass flow rates were directly measured from the sensors while other quantities such as quality, frictional pressure drop and surface roughness and so forth were derived from the raw data. To obtain the uncertainties of the indirectly determined quantities, the uncertainty of measurements should be characterized and correctly quantified.

For all the measurements, the total uncertainty involved the uncertainties from instrument, calibration, and actual sampling processes. Assuming all these three processes are independent and random, in most cases they indeed are, the total uncertainty is written as

$$u_{tot} = \sqrt{u_{instrument} + u_{calibration} + u_{sampling}} \tag{27}$$

The instrument uncertainties, $u_{instrument}$, in Equation (27) are listed in Table A-1 for all the direct measurements.

Table A-1 Instrument Uncertainties

Measured Variable	Instrument	Uncertainty
V_{air}	Alnor Compuflow 8585 Hot-Wire Anemometer	$\pm 3\%$ of reading
$T_{sat,t}$, $T_{sat,b}$, T_{ao}, T_{ai}, $T_{s,}$ T_{amb}	Sheathed T-Type Thermocouple	$\pm 0.05\ K$
T_{wt}, T_{wb}, T_{at}, T_{ab}	Twisted T-Type Thermocouple	$\pm 0.16\ K$
$\Delta P_{gauge,in}$	Rosemount 1151 diaphragm differential pressure transducer, 0-30inH_2O	$\pm 7.0\ Pa$
ΔP_1	Rosemount 1151 diaphragm differential pressure transducer, 0-2inH_2O	$\pm 1.0\ Pa$

Table A-1 Instrument Uncertainties (cont.)

$\Delta P_2, \Delta P_3$	Rosemount 1151 diaphragm differential pressure transducer, 0-1inH_2O	$\pm 0.5\ Pa$
ΔP_4	Rosemount 1151 diaphragm differential pressure transducer, 0-0.5inH_2O	$\pm 0.25\ Pa$
ΔP_5	Rosemount 1151 diaphragm differential pressure transducer, 0-0.35inH_2O	$\pm 0.2\ Pa$
$\Delta P_{gauge,out}$	Fisher 1151 diaphragm differential pressure transducer, 0-30inH_2O	$\pm 7.0\ Pa$
$\dot{m}_s$	Micro-Motion CMF025 mass flow meter	$\pm 0.1\%$ of the rate, g

These instrument uncertainties are the published accuracy of the device based manufacturer's handbook. Calibration uncertainty was only important for air velocity measurement because of the difficulty of calibrating anemometer at low air speed, and the errors from calibrating other instruments were very small. As no explicit equation or information can be used to define the uncertainty of calibration, they were assigned empirically. The sampling uncertainty was defined as the standard measurement error multiplied by a factor of 1.96 for reporting the error within 95% confidence interval:

$$u_{sampling} = \frac{\sigma_s}{\sqrt{n_s}} \times 1.96 \tag{28}$$

Where σ_s is the standard deviation of the sample, and n_s is the sample size. So it is obvious that for the measuring process that is under statistical control, larger sample size would reduce the sampling error.

A.2 Uncertainty of Determined Quantities

For indirectly determined quantities, the uncertainties were affected by the errors from all the intermediate steps and quantities, and can be quantified as

$$u_y = \sqrt{\sum_i \left(\frac{\partial y}{\partial x}\right)^2 u_x^2} \tag{29}$$

in which u_y is the uncertainty of the determined quantity y, u_x is the uncertainty of existing quantity x, and $\sum_i \left(\frac{\partial y}{\partial x}\right)^2$ is the summation of the partial derivatives of y with respect to x. All the uncertainty calculations were performed in MATLAB.

According to the methods proposed by Park et al [43], the combined overall pressure drop as well as the uncertainty associated were determined in the following way:

Firstly, denote the overall pressure drop obtained by subtracting outlet gauge pressure from inlet gauge pressure as $\Delta P_{o,1}$, and the overall pressure drop obtained by summing all five differential pressures up as $\Delta P_{o,2}$. The uncertainties of $\Delta P_{o,1}$ and $\Delta P_{o,2}$ are u_1 and u_2, respectively, and were determined following the steps described in the preceding section. Then, the combined overall pressure drop was calculated as

$$\Delta P_{o,com} = \psi_1 \Delta P_{o,1} + \psi_2 \Delta P_{o,2} \tag{30}$$

where ψ_1 and ψ_2 are the averaging weighted factors defined as

$$\psi_1 = \frac{u_2^2}{u_1^2 + u_2^2} \tag{31}$$

$$\psi_2 = \frac{u_1^2}{u_1^2 + u_2^2} \tag{32}$$

And the uncertainty of the combined overall pressure drop is

$$u_{o,com} = \sqrt{\psi_1 u_1^2 + \psi_2 u_2^2} \tag{33}$$

This method provides the useful tool to statistically combine redundant pressure drop measurements, and is proven to be able to minimize the experimental uncertainty in [43].

Appendix B: Experiment Facility Designs

The majority of the system design works were done and described in detail by Davies [32]. As a supplement to those illustrations, the designs and descriptions of the electric and data acquisition systems that were not introduced in [32] are elaborated here in this chapter.

B.1 Data Acquisition System

To acquire data automatically and continuously, a Keysight® data acquisition and control system, shown in Figure B-1, was used to read signals and send control commands. All the analog signals from 105 thermocouples, 7 pressure sensors, and 1 mass flow meter were connected to a patch panel, shown in Figure B-2, and then routed to the data logger for data recording and processing. To reduce measurement noises, only shielded cables were used as signal wires.

Figure B-1 Keysight 3852A Data Acquisition and Control System

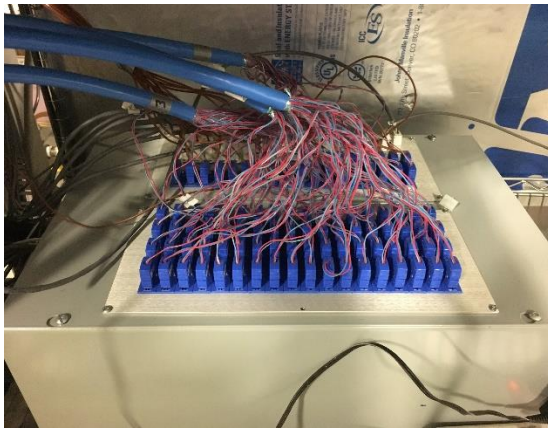

Figure B-2 Patch Panel Box

With the help of LabVIEW, all the measurements were transmitted to the PC for data recording, processing, and displaying in real time. The LabVIEW program also served as an interface to control the heater power through Din-A-Mite.

B.2 Electrical Control System

The design of electric circuit that was responsible for power distribution and control, safety and protection is shown in Figure B-3.

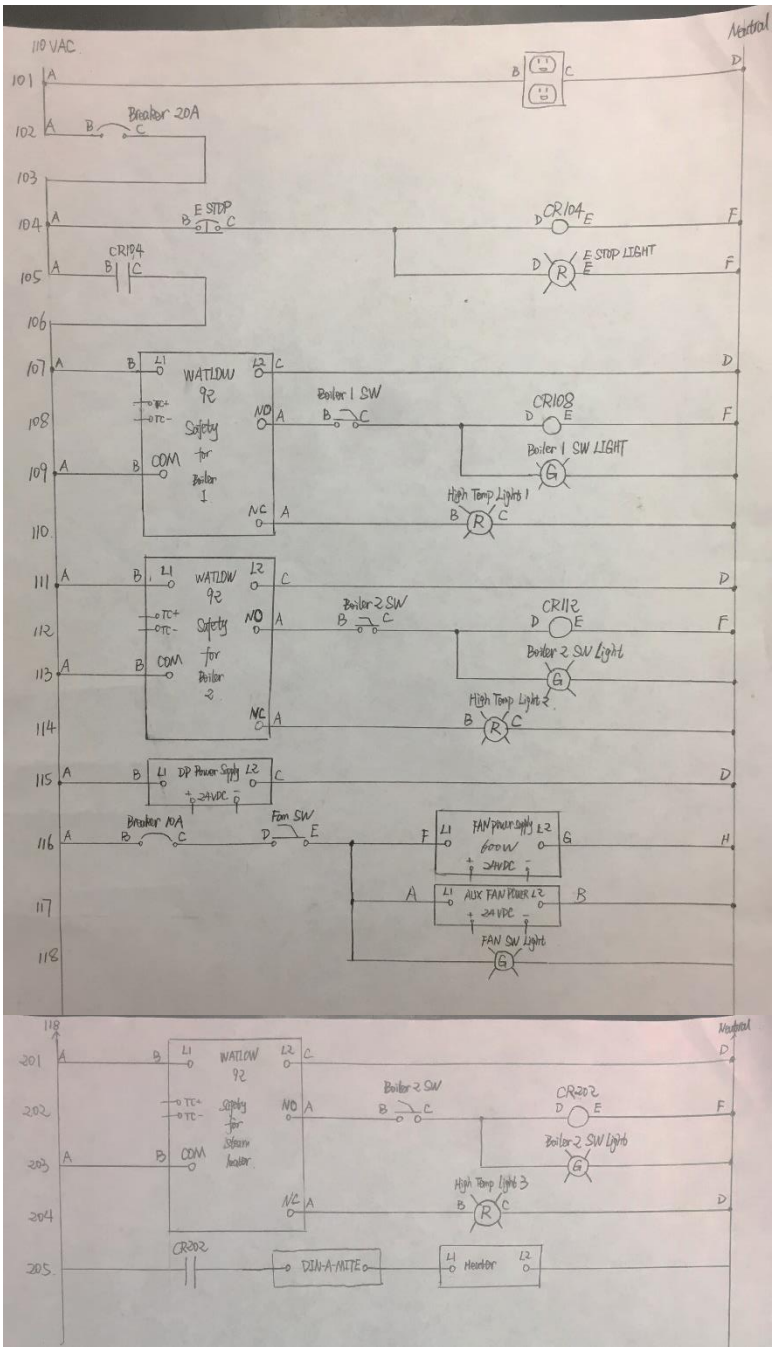

Figure B-3 Low Voltage Circuit Design

The power outlet in rung 101 is uncontrolled and thus used to power PC and data logger. When E-Stop is pressed, all the power connections are cut immediately except the outlet. Other safety features such as overheat protection for heaters and over-amperage breakers were also installed. The actual layout of the electrical panel is shown in Figure B-4.

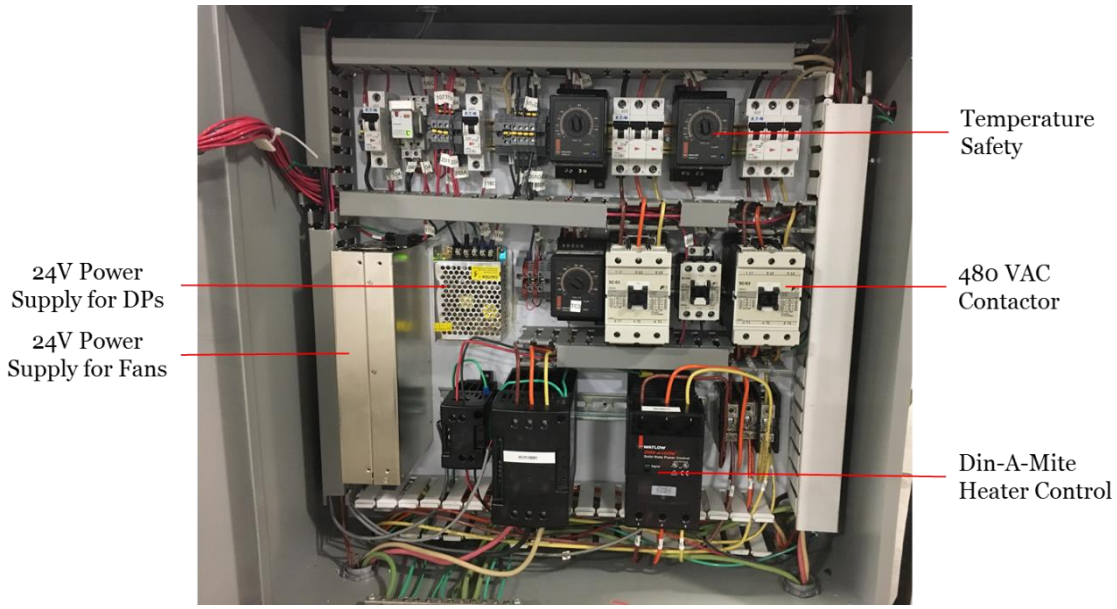

Figure B-4 Electrical Cabinet Layout